BRNO UNIVERSITY OF TECHNOLOGY
VYSOKÉ UČENÍ TECHNICKÉ V BRNĚ

FACULTY OF CHEMISTRY
FAKULTA CHEMICKÁ

INSTITUTE OF MATERIALS SCIENCE
ÚSTAV CHEMIE MATERIÁLŮ

CHARACTERIZATION OF A NEW DEPOSITION SYSTEM FOR COATING THE FIBERS

CHARAKTERIZACE NOVÉHO DEPOZIČNÍHO SYSTÉMU PRO POVLAKOVÁNÍ VLÁKEN

BACHELOR'S THESIS
BAKALÁŘSKÁ PRÁCE

AUTHOR
AUTOR PRÁCE
Milan Zvonek

SUPERVISOR
VEDOUCÍ PRÁCE
prof. RNDr. Vladimír Čech, Ph.D.

BRNO 2016

Brno University of Technology
Faculty of Chemistry
Purkyňova 464/118, 61200 Brno 12

Bachelor Thesis Assignment

Number of bachelor thesis:	**FCH-BAK0971/2015**	Academic year: **2015/2016**
Institute:	Institute of Materials Science	
Student:	**Milan Zvonek**	
Study programme:	Chemistry and Chemical Technologies (B2801)	
Study field:	Chemistry, Technology and Properties of Materials (2808R016)	
Head of thesis:	**prof. RNDr. Vladimír Čech, Ph.D.**	

Title of bachelor thesis:
Characterization of a new deposition system for coating the fibers

Bachelor thesis assignment:
-Background search in plasma-enhanced chemical vapour deposition (PECVD), spectroscopic ellipsometry, and infrared spectroscopy.
-Burning conditions for RF discharge.
-Practical skills in thin film deposition and analytical methods.
-Thin film properties as a function of deposition conditions.

Deadline for bachelor thesis delivery: 20.5.2016
Bachelor thesis is necessary to deliver to a secretary of institute in the number of copies defined by the dean and in an electronic way to a head of bachelor thesis. This assignment is enclosure of bachelor thesis.

- -	- -	- -
Milan Zvonek Student	prof. RNDr. Vladimír Čech, Ph.D. Head of thesis	prof. RNDr. Josef Jančář, CSc. Head of institute

In Brno, 31.1.2016

- -
prof. Ing. Martin Weiter, Ph.D.
Dean

ABSTRACT

The aim of the bachelor thesis is characterisation of a deposition system for coating thin films. The theoretical part focuses on literature recherché on plasma and plasma polymerization, thin films and its analysis using IR spectroscopy and spectroscopic ellipsometry. Experimental part deals with materials and equipment used for preparation of thin films using plasma polymerisation. The final part of the thesis describes the measurement results of the thin films deposition and their evaluation with respect to the deposition conditions.

ABSTRAKT

Cieľom bakalárskej práce je charakterizácia depozičného systému na výrobu tenkých vrstiev. Teoretická časť je zameraná na literárnu rešerš o plazme, plazmovej polymerácií, tenkých vrstvách a ich analýzu pomocou infračervenej spektroskopie a spektroskopickej elipsometrie. Experimentálna časť popisuje použité materiály a aparaturu použitú na prípravu tenkých vrstiev pomocou plazmovej polymerácie. Posledná časť popisuje výsledky merania depozícií tenkých vrstiev a ich vyhodnotenie vzhľadom na depozičné podmienky.

KEYWORDS

Thin film, plasma, plasma polymerization, IR spectroscopy, spectroscopic ellipsometry, tetravinylsilane.

KĽÚČOVÉ SLOVÁ

Tenká vrsva, plazma, plazmová polymerizácia, infračervená spektroskopia, spektroskopická elipsometria, tetravinylsilan.

ZVONEK, M. *Charakterizace nového depozičního systému pro povlakování vláken.* Brno: Vysoké učení technické v Brně, Fakulta chemická, 2016. 40 s. Vedoucí bakalářské práce prof. RNDr. Vladimír Čech, Ph.D..

DECLARATION

I declare that the bachelor thesis has been worked out by myself and that all the quotations from the used literary sources are accurate and complete. The content of the bachelor thesis is the property of the Faculty of Chemistry of Brno University of Technology and all commercial uses are allowed only if approved by both the supervisor and the dean of the Faculty of Chemistry, BUT.

……
student's signature

ACKNOWLEDGEMENT

I would like to thank my supervisor prof. RNDr. Vladimír Čech, Ph.D. for technical leadership, provided consultations and literature during thesis solution. I would also like to thank Ing. Antonín Knob and Ing. Martin Branecký for the help and advice they provided during measurement. Last but not least I would like to thank my family and friends for the support during the study. This work was supported in part by the Technology Agency of the Czech Republic, grant no. TA01010796, and the Czech Science Foundation, grant no. 16-09161S.

CONTENTS

1 INTRODUCTION

Plasma polymerization is a process for formation of new kinds of materials, which differ from conventional polymers and most inorganic materials. This technology is used in many technological branches and has a wide variety of use. Surface modification of materials has been commonly used to alter the adhesion and wettability of materials. Plasma polymers can also be altered to change their conductivity and thus create insulating materials as well as conductors and semiconductors which are used in nanoelectronics. Plasma polymer technology can be used to create functional interlayers for composite materials, where the plasma polymer film (interlayer) connects and strengthens the bond between the matrix and the reinforcement.

This bachelor's thesis focuses on preparation and characterisation of thin films formed by plasma polymerisation with tetravinylsilane (TVS) as used monomer. Deposition apparatus on which the depositions were performed is labelled "A4". Samples were deposited under different deposition conditions to obtain data on behaviour of plasma in the reaction chamber and deposition speed in different positions of the chamber. The obtained data was then evaluated using IR spectroscopy and spectroscopic ellipsometry. Samples were then compared based on the different deposition conditions and different placement inside the reaction chamber.

This thesis serves as a baseline of operations for deposition apparatus "A4" to ensure optimal conditions for depositions of further substrates as well as different types of samples like glass fibres in the future.

2 THEORETICAL PART

2.1 Plasma polymerization

2.1.1 Plasma

Plasma is characterised as a state of matter in which the electrons, positively and negatively charged particles, neutral atoms and molecules coexist in a highly activated state. Characteristics of plasma are high ionisation and very high energy compared to other states of matter such as solid, liquid or gas (Figure 1: Schematic of transition state [1].Figure 1) [1].

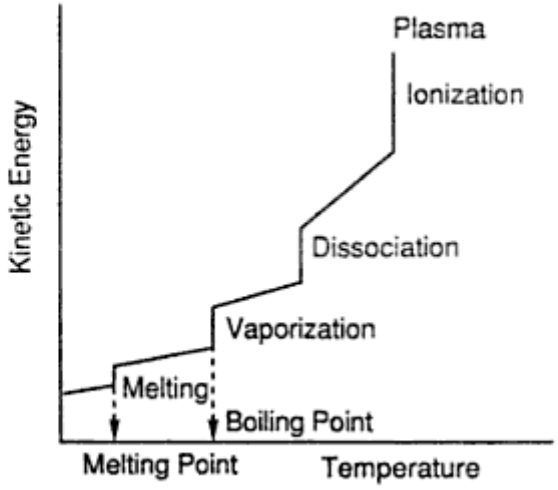

Figure 1: Schematic of transition state [1].

Plasmas are frequently divided according to the temperature into low- (LTP) and high-temperature plasmas (HTP). Further division can be seen in Table 1, where T_e – electron energy in K ($1\,\text{eV} = 11600\,\text{K}$), T_i – ion energy in K and T_g – translational kinetic energy of gas in K [2].

Table 1: Division of plasma [2].

Division of plasma		**Temperature**	**Occurrence**
Low-temperature plasma (LTP)	Thermal LTP	$T_e \approx T_i \approx T_g \lesssim 2\times10^4$ K	arc plasma at normal pressure
	Non-thermal LTP	$T_i \approx T_g \approx 300$ K $T_i \ll T_e \lesssim 10^5$ K	low pressure glow discharge
High-temperature plasma (HTP)		$T_i \approx T_e \gtrsim 10^7$ K	fusion plasmas

The most widely used plasma for PECVD is non-thermal LTP. Due to its high energy of electrons (T_e) and relatively low temperature of the gas (T_g), particles can interact with and activate substrates or reactive gases [3].

One of the main properties of plasma is its quasineutrality. This means that under equilibrium with no external forces present, in a volume of the plasma large enough to contain a large number of particles and yet sufficiently small compared to the characteristic lengths for variation of macroscopic parameters such as density and temperature, the net resulting

electric charge is zero. If a positively or negatively charged particle is placed into plasma, it disturbs the quasineutrality by influencing other particles around itself. This disturbance decreases in magnitude the further away it is from the placed particle until it has no effect. This is caused by Debye shielding, characterised by Debye length, λ_D, which can be considered as a measure of the distance over which fluctuating electric potentials may appear in a plasma. [1, 4]

For plasma to occur it must satisfy the plasma criteria. The first criterion is large enough dimensions of plasma compared to λ_D. If L is a characteristic dimension of the plasma then $L \gg \lambda_D$ must be satisfied. Since the Debye shielding is a result of collective particle behaviour, a large number of electrons is needed within a sphere with radius of the Debye length, therefore a second criterion states

$$N_D = n_e \frac{4}{3} \pi \lambda_D^3 \gg 1, \tag{1}$$

where n_e is the concentration of electrons, N_D is number of charged particles and λ_D is Debye length. [1, 4]

The third criterion is plasma frequency, which is a natural frequency of particle oscillations. This is caused by disturbance in plasma, creation of internal electric field and subsequent movement of electrons towards equilibrium. These electrons move beyond the point of equilibrium and an electric field is produced in the opposite direction. Plasma frequency is given by

$$\omega = \sqrt{\frac{n_e e^2}{m_e \varepsilon_0}}. \tag{2}$$

Ionised gas can be considered plasma only when $\omega\tau > 1$, where τ states the average time an electron travels between collisions with neutral particles and ω represents the angular frequency of typical plasma oscillation. [4]

2.1.2 Mechanism of plasma polymerization

Plasma polymerization is a thin film-forming process in which the film is deposited directly on surface of the substrate without any fabrication. This process causes the growth of low-molecular weight monomers into high-molecular weight polymers. Plasma polymerization differs greatly from conventional polymerization in the product of the polymerization, its structure, physical and chemical properties. The oxygen incorporation into the plasma polymer may occur due to residual air in the reaction chamber. Plasma is the source of energy and initiator, which activates the electrons, ions and radicals of the monomer [1]. The most suitable plasma for this process is the non-thermal LTP [5].

The mechanism of plasma polymerization implements elemental reactions occurring in plasma, which are the fragmentation of monomer molecules, the formation of active sites (radicals) and recombination of the activated fragments. The plasma polymerization does not require polymerizable bonds such as double bond, triple bond or cyclic structure. The propagation reaction in plasma polymerization is a stepwise reaction of recombination between biradicals that are formed from fragmentation of the starting molecules by plasma. Due to this effect, it is possible that the sequence of molecules after the polymerization is

different than of the starting molecules [1, 3]. The scheme of plasma polymerization is illustrated in Figure 2.

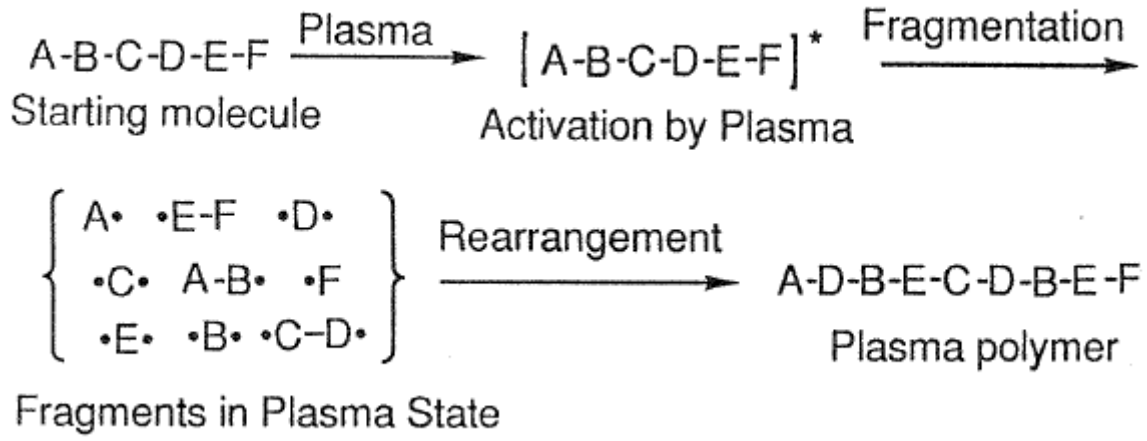

Figure 2: Schematic of presentation of plasma polymerization [1].

The fragmentation of starting molecules in plasma is represented by two types of reactions: the elimination of the hydrogen atom and the C – C bond scission (Figure 3).

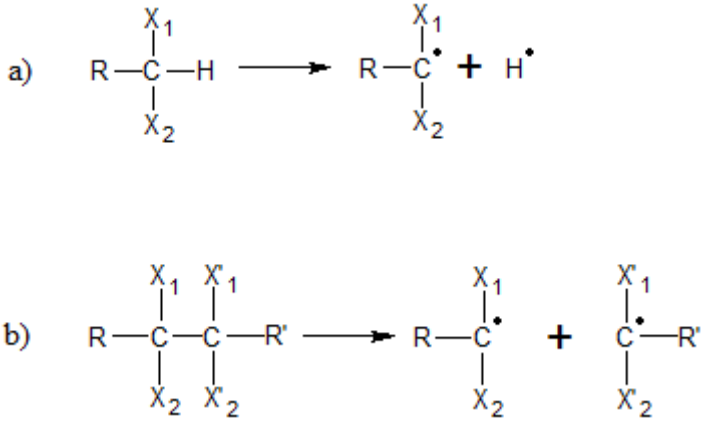

Figure 3: Schematic of hydrogen elimination (a) and C – C bond scission (b) [1].

Hydrogen elimination is considered to contribute greatly to the polymer-forming process in plasma polymerization.

It seems probable that hydrogen atoms are eliminated from monomer molecules by plasma to form monoradicals $M_i^{\bullet}$ and biradicals ${}^{\bullet}M_k^{\bullet}$, and the addition of the radicals to monomer and the recombination between two radicals proceed to make large molecules with or without radical. Figure 4 shows the polymer-forming process in plasma polymerization. Monoradical $M_i^{\bullet}$ adds to the monomer to form a new radical $M_j^{\bullet} - M^{\bullet}$ (reaction a). Monoradical $M_i^{\bullet}$ can also recombine with monoradical $M_j^{\bullet}$ to form a neutral molecule $M_i - M_j$ (reaction b) or recombines with biradical ${}^{\bullet}M_k^{\bullet}$ to form a new monoradical $M_i - M_k^{\bullet}$ (reaction c). Biradical ${}^{\bullet}M_k^{\bullet}$ adds to monomer to form a new biradical ${}^{\bullet}M_k - M^{\bullet}$ (reaction d). Biradical ${}^{\bullet}M_k^{\bullet}$ recombines with biradical ${}^{\bullet}M_j^{\bullet}$ to form a new biradical ${}^{\bullet}M_k - M_j^{\bullet}$ (reaction e). The new neutral molecule $M_i - M_j$ is again activated by plasma to form mono- or biradicals and cycle

I repeats. The new monoradicals $M_i - M_k^{\bullet}$ and biradicals $^{\bullet}M_k - M_j^{\bullet}$ further recombine to form larger radicals in cycle II [1].

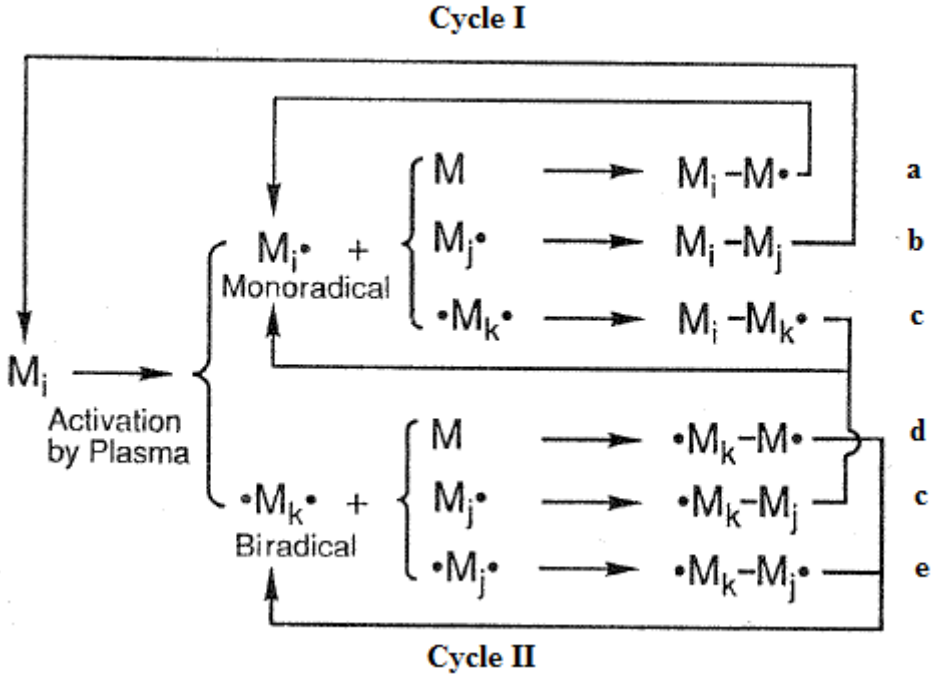

Figure 4: Overall plasma polymerization mechanism [1].

2.1.3 Thin film

Thin films are formed by the deposition of individual atoms on a substrate. A thin film is defined as a low-dimensional material created by condensing, one-by-one, atomic, molecular or ionic species of matter. It can be also defined by S/V surface to volume ratio which satisfy the condition that $|S/V| >> 6$ (Figure 5). Thin films differ from bulk materials in their physical properties. In general, the thickness of a thin film is $0.1\,\text{nm} - 10\,\mu\text{m}$ [6].

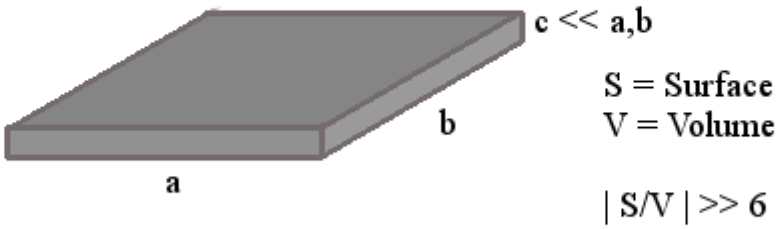

Figure 5: Model of thin layer.

The basic properties of film, such as film composition, crystal phase and orientation, film thickness and microstructure are controlled by deposition conditions. Thin films have unique properties that cannot be observed in bulk materials. These are unique material properties resulting from atomic growth process and size effects, including quantum size effects, characterised by the thickness, crystalline orientation and multilayer aspects. [6]

There are two dimensional phenomena. Classical dimensional phenomenon can be observed, if the film thickness is comparable to the mean of electrons or if the film thickness is comparable to the radius of electron in magnetic field in the case of galvanomagnetic phenomena. Quantum dimensional phenomenon can be observed in crystalline film, if the film thickness is comparable to the de Broglie wavelength of electron.

Thin films can be formed by inorganic, organic or hybrid materials in a form of crystalline, semicrystalline or amorphous materials. With respect to electrical conductivity, the thin films can be superconductive, conductive, semiconductive or dielectric.

Thin films have been used in many types of engineering systems and have been adapted to fulfill a wide variety of functions such as the use of surface coatings to protect structural materials in high temperature environments for example in gas turbine engines. Thin films are integral parts of many micro-electro-mechanical systems designed to work as sensors or actuators. Extending the durability of components by the use of surface coatings or surface treatments is another use of thin films and can be seen in internal combustion engines, artificial hip and knee implants and computer hard disks for magnetic data storage [7].

2.1.4 Operational parameters of plasma polymerization

When the monomer gains enough energy from plasma, it is fragmented into smaller, highly activated molecules. These molecules merge together to form larger molecules which are deposited onto the surface of a substrate. After the polymers are deposited, they are continuously irradiated by the plasma. In such conditions, the deposited polymers deteriorate and their chemical structure is changed. This change is caused by the simultaneous deposition and ablation of the polymer on the substrate (Figure 6). The process of ablation and polymerization has competitive character [1].

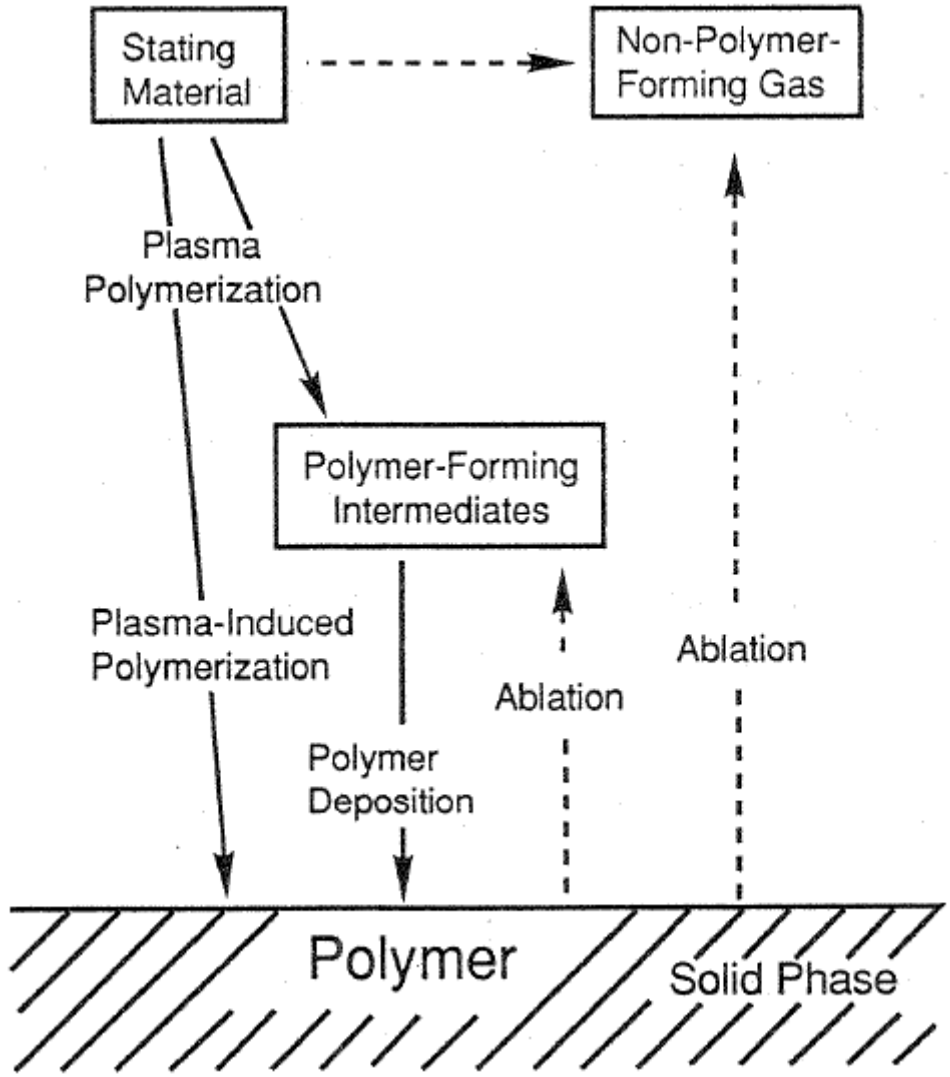

Figure 6: Overall reactions of plasma polymerization [1].

From the viewpoint of plasma polymerization as a material production process, there coexist two opposing processes: polymer formation, which leads to the deposition of material, and ablation, which leads to the removal of material. The activation of monomers and reactivation of the recombined molecules is due to fragmentation by plasma. The fragmentation process depends on how much of electric energy was used to maintain plasma, how much the monomer was added into plasma and where the monomer molecules interacted with activated species of the plasma. Therefore, a controlling parameter of W/FM (W – power of generator [W], F – monomer flow rate $[\,\mathrm{mol}\cdot\mathrm{s}^{-1}]$, M – molecular weight of the monomer $[\,\mathrm{kg}\cdot\mathrm{mol}^{-1}]$) was introduced to control the process of plasma polymerization. The magnitude of W/FM parameter is considered to be proportional to the concentration of activated particles in plasma. The polymer deposition rate increases with increasing W/FM parameter under the operational condition, where the activated species have considerably lower concentration than monomer molecules in plasma. Such conditions refer to monomer sufficient region (Figure 7). Afterwards the polymer formation rate levels off in the competition region and with the increasing W/FM parameter the polymer formation rate decreases due to lack of monomer molecules, these conditions refer to monomer deficient region. In the monomer sufficient

region, monomer molecules are subjected to less fragmentation to be plasma-polymerised. In the monomer-deficient region, the monomer molecules are subjected to heavy fragmentation and plasma polymers with great rearrangement are formed. The ideal conditions for plasma polymerization are in the competition region, where the deposition rate is the highest [1, 3].

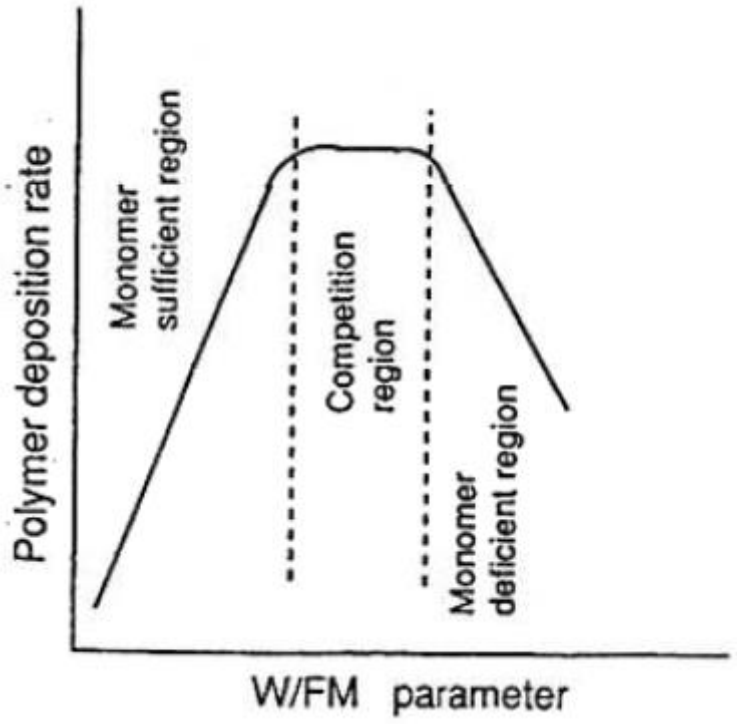

Figure 7: Domain of plasma polymer deposition [1].

2.1.5 Organosilicon plasma polymers

The organosilicon polymers are molecules, whose monomers consists of silicon atom and organic groups where atoms of carbon, oxygen, nitrogen and hydrogen can be found. The first reason for the development is because of the focus on plasma processes in the seventies and advancement in micro-electronic technologies. These technologies concern principally the silicon and silicon-based materials (SiO_2, Si_3N_4…). The organosilicon precursors are used for the deposition of these products. The second main reason is that the films made from organosilicons have remarkable optical, mechanical and electrical properties which resulted in the development of their applications in the fields of protective coatings, scratch resistant films, planar light guides, dielectric films for capacitors or intermetallic insulation in integrated circuits. The organosilicon precursors are in general stable, non-toxic and commercially available [8].

Monomers mostly used are Hexamethyldisiloxane (HMDSO) and Tetraethoxysilane (TEOS) and Hexamethyldisilazane (HMDSN), which contains two Si-N bonds. These monomers are mostly used in mixtures with rare gas such as Argon and also with an active gas like O_2 or N_2O. It is generally admitted that the atomic oxygen is created during the plasma phase and that this atomic oxygen reacts in the gas and at the plasma surface interface with organic parts of the organosilicon precursor. The mostly commonly used organosilicon precursors are in Table 2 [8].

Table 2: Main organosilicon precursors and conditions used to growth plasma films [8].

Name and shortcut	Plasma source	Pressure range	Power range	Reference
Hexamethyldisiloxane HMDSO	RF, μW, LF	10^{-1} – 10^{2} Pa	3–100 W	[9, 10, 11, 12, 13]
Tetraethoxysilane TEOS	RF, μW,	10^{-1} – 10^{2} Pa	3–100 W	[14, 15, 16, 17]
Tetramethyldisiloxane TMDSO	13,56 MHz, Inductive coupling	1.3 Pa	25 W	[18]
Divinyltetramethyldisiloxane DVTMDSO	13,56 MHz, Capacitive coupling remote plasma	1–10 Pa	14–200 W	[19]
Methyltrimethoxysilane TMOS	13,56 MHz, Parallel plate	14.7 Pa	300 W	[20]
Octamethylcyclotetrasiloxane OMCATS	13,56 MHz, Capacitive coupling remote plasma	1–10 Pa	14–200 W	[19]
Bis(Trimethylsilyl)methane BTMSM	13,56 MHz, inductive coupling	1.3 Pa	50–150 W	[21]
Hexamethyldisilane HMDS	13,56 MHz, inductive coupling	1.3 Pa	50–150 W	[21]
Tetramethylsilane TMS	13,56 MHz, Inductive coupling	1.3 Pa	25 W	[18]
Tetravinylsilane TVS	13,56 MHz helical coupling	0.1–4.4 Pa	0.05–10 W	[22]

2.2 Thin film analysis

There are many ways to collect information about thin films and different techniques were designed based on characteristics that needed to be analysed. These techniques can be divided into film thickness, structural characterisation and chemical characterisation. Methods used in this thesis are IR spectroscopy, for its ability to recognise structural groups, and spectroscopic ellipsometry, for the optical characterisation and film thickness.

2.2.1 IR spectroscopy

IR spectroscopy is very important because of the high information content of a spectrum and because of its variety of possibilities for sample measurement and substance preparation.

Therefore, IR spectroscopy has become one of the most important analytical methods for preparative as well as analytical chemistry. The possibility of directly stating the structural groups, which is often very difficult or cannot be derived by other methods, constitutes the essence of IR spectroscopy and substantiates it as one of the most important methods in instrumental analysis. The position and intensity of absorption bands of a substance are very specific to that substance. The IR spectrum is highly characteristic for a substance and can be used for identifying it. The high specificity is based on the good reproducibility with which the coordinates of the absorption maxima can be measured. In addition, two factors are important for successful substance identification through IR spectrum: The generally high number of absorption maxima occurrence and large number of comparative IR spectra previously measured [23].

If I_0 is the intensity of monochromatic radiation entering a sample, and I is the intensity transmitted by the sample, then the ratio I / I_0 is called the transmittance (T) of the sample. If the sample cell (thin film) has thickness *b* and the absorbing component has a concentration of *c*, and the constant *a* refers to the absorptivity, the fundamental equation concerning the absorption of radiation is

$$T = I / I_0 = 10^{-abc}, \tag{3}$$

This equation can be transformed and a new symbol A – absorbance is used

$$A = \log_{10}(I_0 / I) = abc, \tag{4}$$

The absorption law is called Bouguer-Lambert-Beer law and two conditions are implied using this equation: The first is that the resolution element being measured is monochromatic which means that the region of spectrum that is measured must have a small spread of wavelengths. The second condition is, that the absorptivity *a* must be constant throughout different concentration values. [23]

Electromagnetic radiation is characterised by its wavelength λ, frequency v, and wavenumber $\bar{v}$. The wavenumber expressed in cm^{-1} is the number of waves in a 1 cm long wavetrain. The relation between wavenumber and other units is

$$\bar{v} = \frac{v}{c}, \bar{v} = \frac{1}{\lambda}, \tag{5}$$

where *c* is the velocity of light, v is the frequency in Hz and λ is the wavelength in cm [24].

The infrared region of electromagnetic spectrum covers wavelengths from 800 nm to 1 mm and this region is generally divided into three: near IR (NIR) from the visible to 2.5 μm. Mid IR, from 2.5 to 25 μm and far IR (FIR) from 25 μm to 1 mm. The crucial thing about this division is that most fundamental molecular vibrations occur in the mid IR, making this region the richest in terms of chemical information [25].

When a molecule absorbs radiation energy, it increases its own vibrational energy. In a spectrometer, the molecule is irradiated with a range of infrared frequencies but is only able to absorb radiation energy at certain specific frequencies which matched with the natural vibrational frequencies of the molecule. These frequencies occur in the infrared region of the electromagnetic spectrum. In order to absorb infrared radiation, a molecular vibration must cause a change in the dipole moment of the molecule (Figure 8). The more the dipole moment changes during a vibration, the more easily the photon electric field will activate the vibration.

If a molecular vibration causes no change in the dipole moment, then a forced dipole oscillation cannot activate the vibration [24].

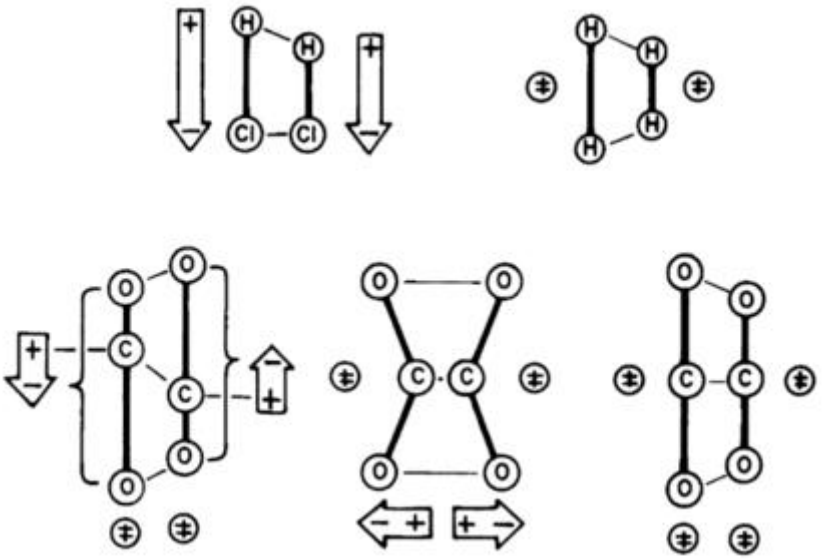

Figure 8: Dipole moment changes in certain molecular vibrations [24].

Two most common spectrometers are dispersive and Fourier transform (FT-IR) spectrometer. The FT spectrometer has several advantages over dispersive and thus has almost entirely replaced the dispersive spectrometer. The disadvantages of the dispersive spectrometer are its high number of moving parts inside spectrometer and their deterioration over time, disruptive effect of scattered light and the increase of temperature of sample caused by the short distance between sample and the source of radiation. This could also cause the sample to break down and emit light, which caused the data to be more inaccurate. The most advantageous feature of FT spectrometer is that radiation from all wavelengths is measured simultaneously, which tremendously decreased the time needed to scan the spectrum. The resolution of the FT spectrometer is generally higher and it is relatively easy to change spectral range of the spectrometer [25, 26].

2.2.2 Spectroscopic ellipsometry

Ellipsometry is an optical measurement technique that characterizes light reflection of a sample. The key feature of ellipsometry is that it measures the change in the polarized light upon light reflection on a sample. The name ellipsometry comes from the fact that polarized light becomes elliptical upon light reflection. Ellipsometry measures two values, which represent the amplitude ratio ψ and phase difference Δ between light waves known as p- and s-polarized light waves. The measurement is performed by polarizing the incident light beam, reflecting it off a smooth sample surface at an oblique angle and then repolarizing the light beam before the intensity of the light beam is measured [25, 27].

Spectroscopic ellipsometry is used to evaluate optical constants and thin film thicknesses of samples, real-time monitoring of the thin film growth and also process diagnoses including etching and thermal oxidation [27].

Ellipsometry experiments produce data that is not useful by itself, computers must be used to evaluate the data and obtain useful quantities such as thin film thickness or optical

functions of materials. The advancement of computer science has enabled the invention of several spectroscopic ellipsometers and the creation of more realistic analysis programs needed to understand and process spectroscopic ellipsometry data [25].

An ellipsometer consists of a light source, a polarization state generator (PSG), a sample, a polarization state detector (PSD), and a light detector. The light source can be a monochromatic (laser) or a white light source (xenon lamp). The PSG and PSD are optical instruments that change the polarization state of light passing through them and they contain optical elements such as polarizers, retarders and photoelastic modulators. Spectroscopic ellipsometers use white light source and a monochromator to select out a specific wavelength. Ellipsometers measure only the characteristics of light reflected or transmitted through the sample (Figure 9). Ellipsometers do not measure the film thickness or optical functions of the materials, they only provide the data, which can be processed to obtain the desirable information about the sample [25].

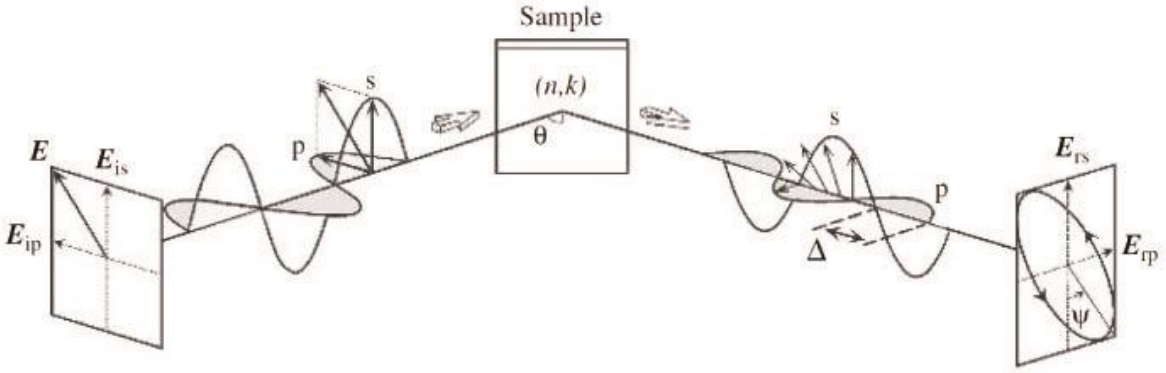

Figure 9: Measurement principle of ellipsometry [27].

There are several types of ellipsometers. One of the oldest types is the nulling ellipsometer. The light source of a nulling ellipsometer is usually a small laser. The PSG is a polarizer-retarder pair and the PSD is a linear polarizer, also called analyser. The nulling ellipsometry is one of the simplest ellipsometers is able to make accurate measurements with proper calibration. One of the disadvantages of this type of ellipsometer is its measurement times are slow and therefore it is not viable for fast time-resolved measurements [25].

The rotating analyser ellipsometer (RAE, Figure 10) is a type of spectroscopic ellipsometer with physically rotating analyser, making the light intensity at the detector a periodic function of time. The measurement time of this type depends only on the speed at which the analyser rotates. If the mechanical parts of the rotating analyser are worn down, it can decrease the precision of acquired data [25].

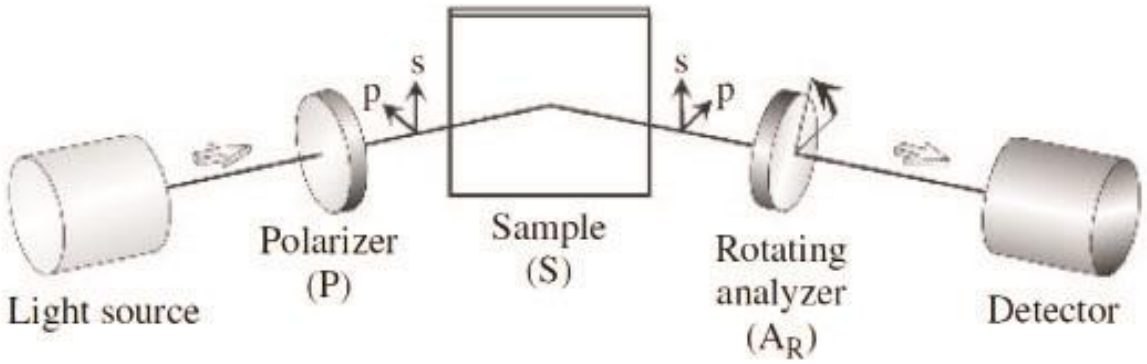

Figure 10: Rotating analyser ellipsometry [27].

Photoelastic modulator ellipsometer (PME, Figure 11) contains a transparent quartz bar which under mechanical strain or electrical signal, it induces a periodical birefringence into the quartz bar. When polarized light goes through the modulator, it is affected by the modulated birefringence resulting in the two components undergoing a modulated phase shift. The linearly polarized beam is transformed into elliptically polarized at the output of the modulator and the size of the ellipse is modulated at the frequency of modulation. This modulation is performed without any mechanical movement which increases the accuracy and signal stability [28].

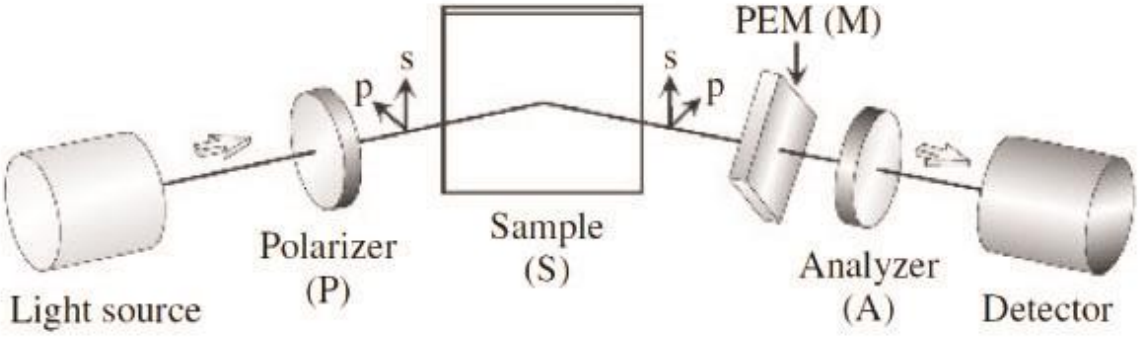

Figure 11: Photoelastic modulator based ellipsometry [27].

3 EXPERIMENTAL PART

3.1 Used materials

Monomer: Tetravinylsilane(TVS, Figure 12), $Si\text{-}(CH=CH_2)_4$, produced by Sigma Aldrich

Molecular weight: 136.27

Density: $0.8\,g\cdot cm^{-3}$

Boiling point: 130°C

Refractive index: 1.461

Purity: 97%

CAS-number: 1112-55-6

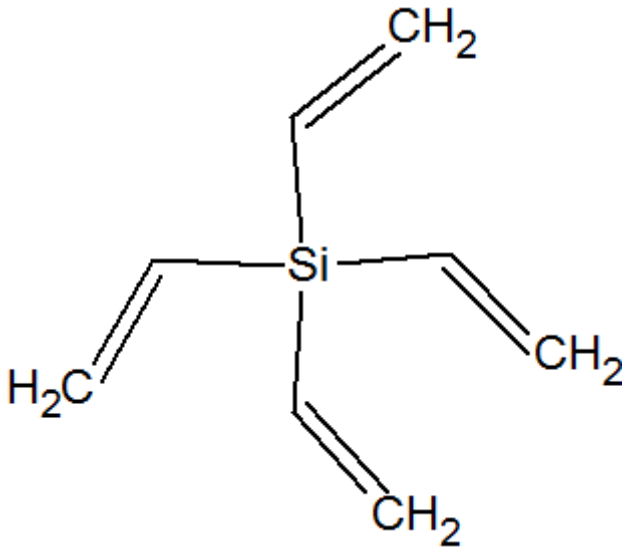

Figure 12: Structural formula of Tetravinylsilane.

Used gases:

Argon is used as a cleaning medium of the reaction chamber and as an inert atmosphere for quenching of free radicals in the reaction chamber after the deposition. The Argon 5.0 with 99.999% purity is used, produced by company Linde gas.

Oxygen is used for pre-treatment of substrates to remove surface contamination and activate surface states. The Oxygen 4.5 with 99.995% purity is used, produced by company Linde gas.

Infrared-transparent double polished silicon wafers (ON Semiconductor Czech Republic s.r.o.) with dimensions 10 × 10 × 0.6 mm are used as planar substates. They are also required in IR spectroscopy and ellipsometry measurements.

3.2 Deposition apparatus

Apparatus "A4" (Figure 15) consists of two main parts: vacuum system, which creates desired pressure inside the reaction chamber and deposition system, which is responsible for optimal plasma discharge in the reaction chamber.

3.2.1 Vacuum system

The pumping system in comprises a turbomolecular pump (Pfeiffer Vacuum) HiCube 80 Eco (Figure 13) with pumping speed for N_2 of $67\,l\cdot s^{-1}$ with backing pump MVP 015 with

pumping speed of $0.5\,\mathrm{m}^3\cdot\mathrm{h}^{-1}$. The operating frequency of the turbomolecular pump is 1500 Hz and it is able to create vacuum of 10^{-5} Pa. The vacuum system is incorporated with a series of gauges, namely Pfeiffer Vacuum Compact Fullrange gauge PKR-251 with measurement range of 10^{-7} – 10^{5} Pa, Pfeiffer Vacuum CMR-364 with measurement range 10^{-2} – $1.1\cdot10^{2}$ Pa and 0.2% accuracy, Pfeiffer Vacuum Compact Pirani gauge TPR-280 with measurement range $5\cdot10^{-2}$ – 10^{5} Pa. The system is equipped with pneumatic valves Pfeiffer vacuum D-35614 Asslar AVC 016 PA with maximum operating pressure of $2\cdot10^{5}$ Pa and AP Tech Diaphragm valves for high purity type AP3540 and AP4540 with maximum operating pressure of $9\cdot10^{5}$ Pa. Mass flow meters are used for each of the working gases as well as monomer. The Low-ΔP-Flow mass flow meters of type F-201CV and F-201DV with operating pressure of 10^{3} Pa and maximum flow speed 100 $\mathrm{ml_n}\cdot\mathrm{min}^{-1}$.

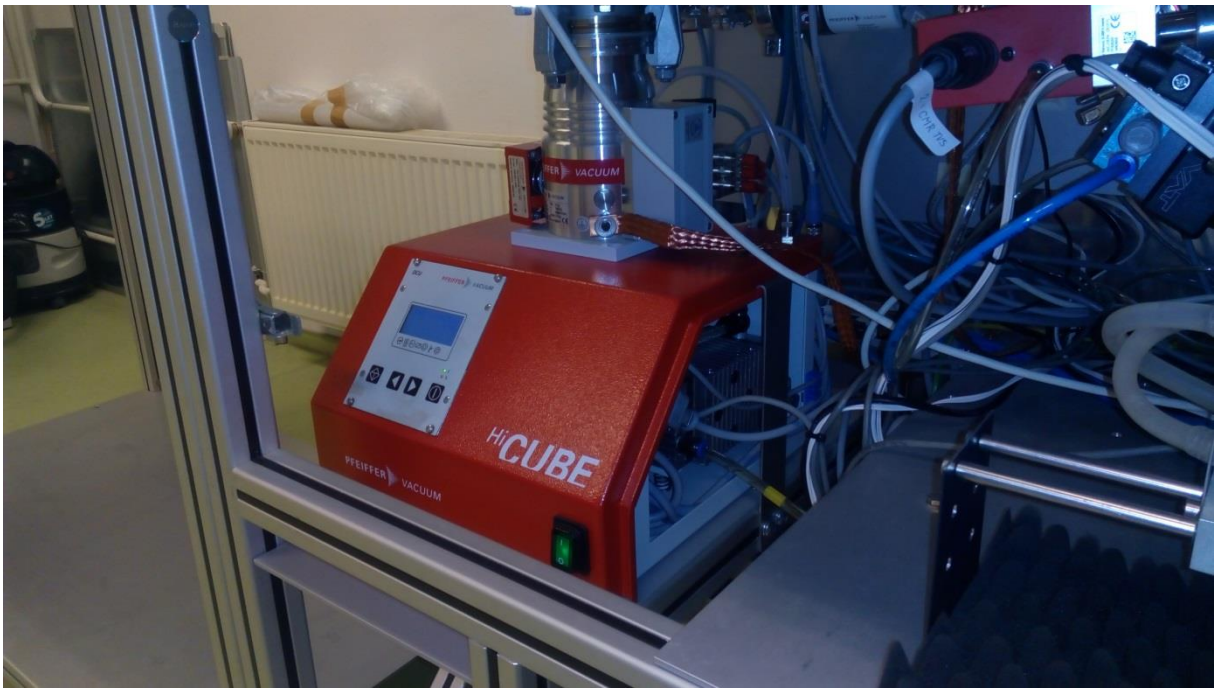

Figure 13: Turbomolecular pump HiCube 80 Eco.

3.2.2 Deposition system

Deposition system (Figure 15) was designed for preparation of thin films for planar substrates as well as fibre coating. The reaction chamber is made of glass tube with diameter of 4 cm and length of 1 m. Throughout the whole length of reaction chamber (Figure 14), there are 7 live electrodes and 8 grounding electrodes alternating one after the other to ensure plasma discharge along the tube.

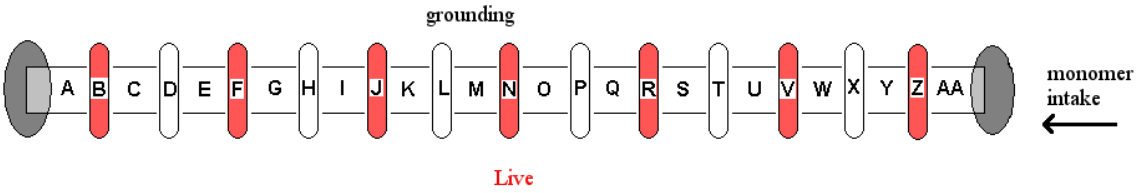

Figure 14: Reaction chamber scheme with labelled positions.

All valves are controlled through PC, flow meters are operated manually. The monomer is placed in a small vial, which is kept in a thermostat at a constant temperature of 15.0 ± 0.1°C.

The glow discharge is powered by Cesar 1310 RF Generator (Advanced Energy) with frequency of 13.56 MHz with maximum power output of 1000 W into a 50 Ω load. The RF generator is controlled manually. It is able to work both in pulsed and continuous wave regimes. The principle of pulse regime is in alternation between intervals, when the discharge is on (t_{on}) and when the discharge is off (t_{off}). The effective power is defined as:

$$P_{eff} = P_{total} \frac{t_{on}}{t_{on} + t_{off}}. \tag{6}$$

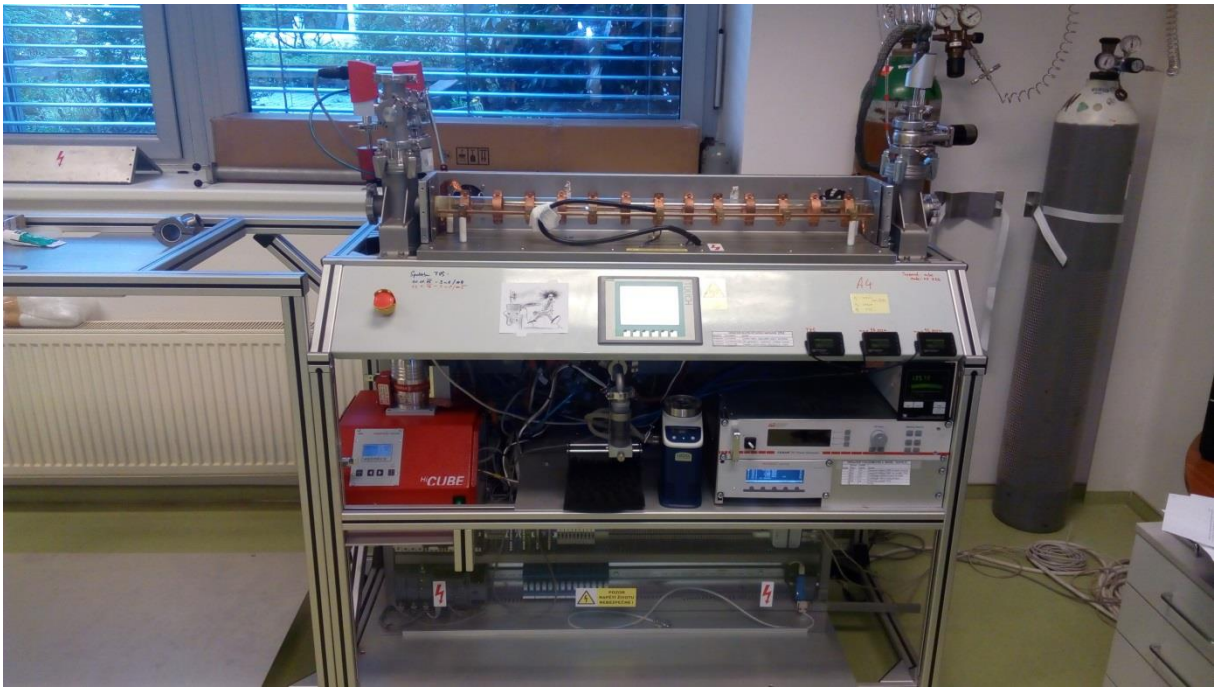

Figure 15: Deposition apparatus “A4”.

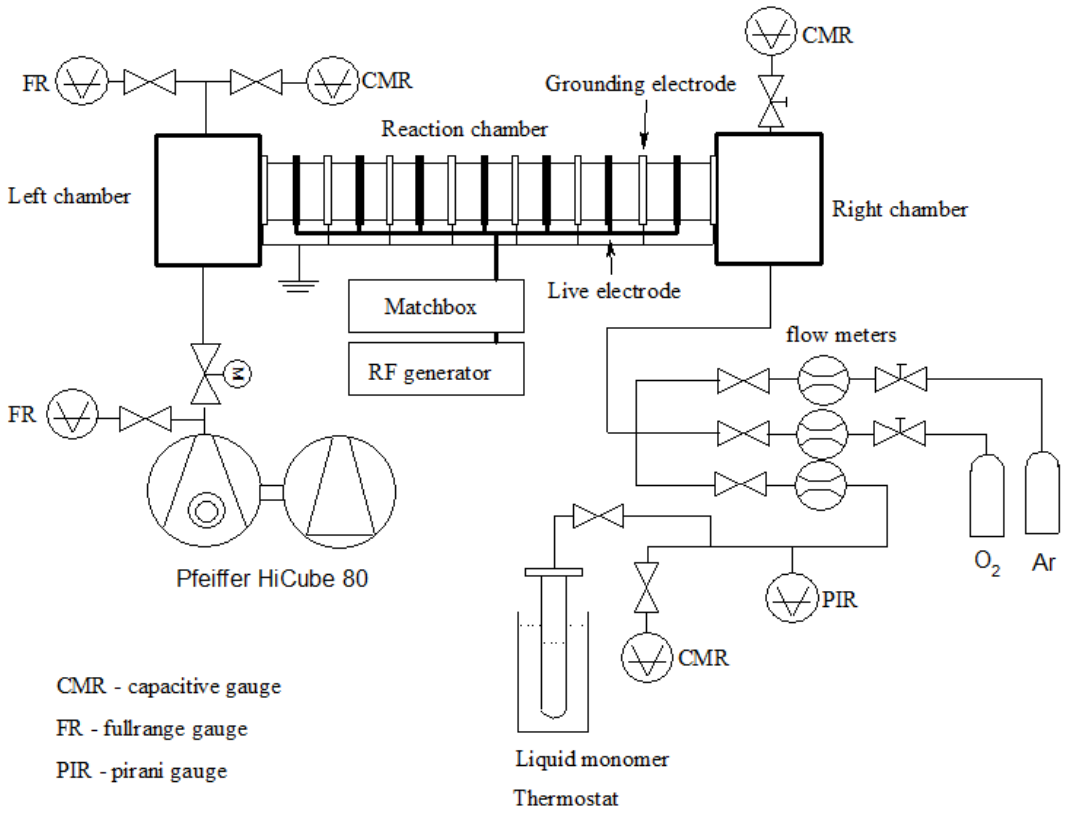

Figure 16: Schematic illustration of deposition apparatus "A4".

3.3 Procedures for plasma polymer film preparation

Table 3: Procedures for plasma polymer film preparation.

1.	A sample was placed into the reaction chamber. The reaction chamber is then shut off the outer atmosphere and turbomolecular pump is turned on to establish vacuum of $2 \cdot 10^{-4}$ Pa .
2.	Oxygen pre-treatment : 1. set Ar flow meter to 10 sccm at 5.7 Pa (left CMR) 2. set Ar flow meter to 0 sccm, set O_2 flow meter to 10 sccm 3. set rf generator to 30 W for 10 minutes
3.	Reservoir with monomer: Release the accumulated monomer vapour to the pressure of 1000 Pa.
4.	Deposition 1. set desired TVS flow rate(29 sccm N_2 = 4.05 sccm TVS) and pressure 2. set rf generator to desired power (10;30;100 W) 3. after the deposition turn off rf generator and close TVS valve.
5.	Post-deposition treatment: 1. fully open main VAT valve 2. set Ar flow meter to 10 sccm for 1 hour
6.	The samples are kept in vacuum for 1 day and then the turbomolecular pump is shut down and samples are collected.

3.4 Thin film analysis apparatus

3.4.1 IR spectrometer

For measuring IR spectra a FT-IR spectrometer Vertex80v (Bruker Optics) was used and operated at vacuum applying a pressure of 160 Pa and with standard optical components: KBr beamsplitter, DLaTGS detector and MIR source, which is able to achieve spectral range of middle IR: 8000 to 350 cm^{-1}. It is based on UltraScan^{TM} interferometer, providing high spectral resolution. The spectrometer is able to eliminate atmospheric moisture absorptions, increasing the sensitivity and stability of the spectrometer. The Bruker Optics DigiTectTM technology prevents external signal disturbance, providing great signal-to-noise ratio. The device is also equipped with functions such as AAR (Automatic Accessory Recognition), ACR (Automatic Component Recognition) as well as permanent online checking (Perfomance Guard). The spectrometer can be also equipped with different optical components to cover the spectral range from the far IR, through mid and near IR to visible up to ultraviolet spectral range. [29]

The device has separate chamber for samples and for optical components, allowing the samples to be inserted without breaking the vacuum and contaminating the optical components. All functions of the spectrometer are controlled via PC using specific software OPUS (Figure 17). In the software, it is needed to select corresponding experiment before the start of the measurement. After an experiment is loaded, it is necessary to measure background noise by choosing the background single channel in the measurement menu. After the background channel is scanned, it is possible to measure a sample with the sample single channel option in the measurement menu. When the sample spectrum is acquired it can be now processed using software tools such as water compensation, cut and subtraction to get optimal results. It is necessary to subtract the absorption spectrum of silicon substrate using the measurement of undeposited silicon wafer to obtain the absorption spectrum of the thin film. The samples were measured in range from 700 to $4000\ cm^{-1}$ with a resolution of $4\ cm^{-1}$.

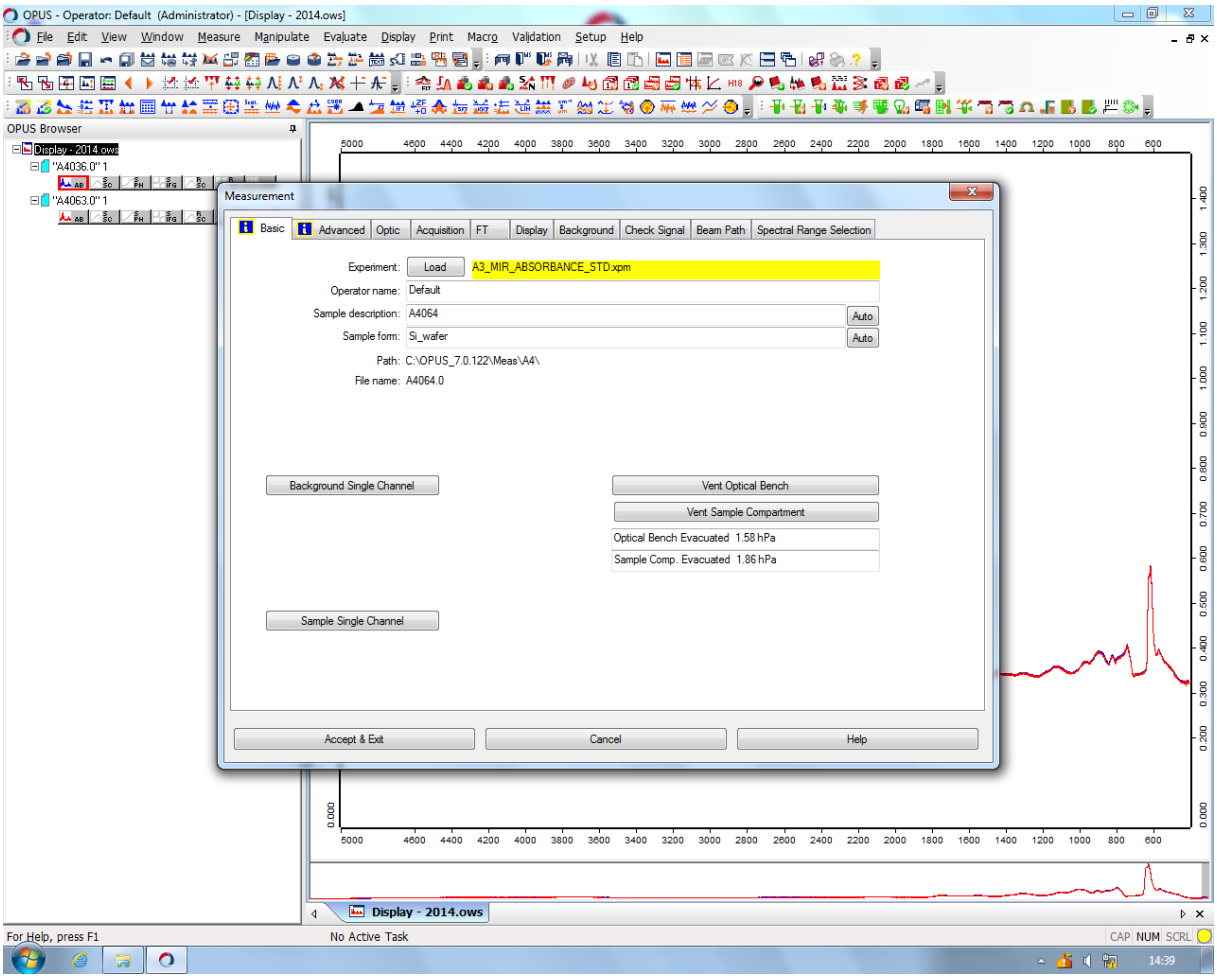

Figure 17: Software OPUS measurement environment.

3.4.2 Spectroscopic ellipsometer

The planar samples were analysed on a spectroscopic ellipsometer UVISEL from company Horiba Jobin-Yvon. The ellipsometer consists of the light source (xenon lamp, 75W), the polarizer, the analyser, the photo-elastic modulator, the monochromator, the multi-channel spectrograph and the operating computer.

The light emitted by the xenon lamp passes through optical fibres into the polarizer, where the light is polarized and focused at sample at a constant angle of 70°. The light beam is then reflected off the sample into the modulator head, which directs the light through photoelastic modulator and analyser. This resulting light signal is then carried through optical fibres to the FUV 200 monochromator or MWL (multi-wavelength) spectrograph, where the light signal is processed and delivered to software DeltaPsi 2 (Figure 18) for further processing.

The sample is fit to a model which corresponds to the deposition conditions and a new model is created and stored in the model library for later use. Model library, together with library of materials is necessary for optimal and accurate ellipsometric measurement.

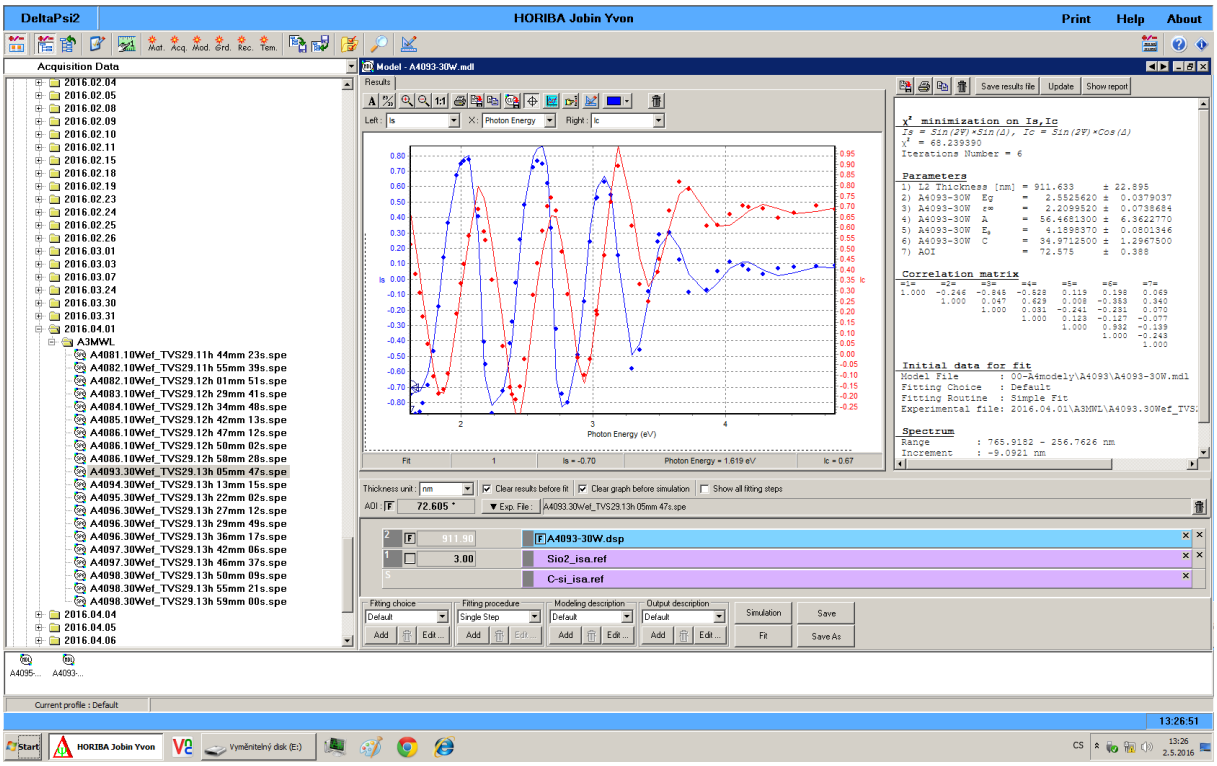

Figure 18: Software DeltaPsi2, sample model creation screen.

The ellipsometric spectra of samples were acquired in a spectral range of 250-830nm with 5 nm increment. The dispersion dependence of the dielectric function was fitted using the five-parametric Tauc-Lorentz formula, which has been derived for the parameterization of the opto-electronic response of amorphous dielectrics. It is based on the Tauc expression for the imaginary part of the dielectric function above the band edge and classic Lorentz oscillator model. The imaginary part of the dielectric function $\varepsilon_2(E)$ in the Tauc-Lorentz expression is parameterized using four parameters – the product of the oscillator amplitude and Tauc constant A_T, the broadening term Γ, the peak transition energy E_0, and the optical band gap E_g:

$$\varepsilon_2(E)=\begin{cases}\left[\dfrac{A_T E_0 \Gamma (E-E_g)^2}{\left[(E^2-E_0^2)^2+\Gamma^2 E^2\right]E}\right] & E>E_g \\ 0 & E\le E_g\end{cases}, \tag{7}$$

The real part of the dielectric function is obtained by Kramers-Kronig integration

$$\varepsilon_1(E)=\varepsilon_1^{\infty}+\frac{2}{\pi}P\int_{E_g}^{\infty}\frac{\zeta\varepsilon_2(\zeta)}{\zeta^2-E^2}\mathrm{d}\zeta, \tag{8}$$

where P stands for the Cauchy principal part of the integral and an additional fitting parameter ε_1^{∞} has been included. For optical characterisation of the films, a suitable parameterization of the material optical constants and realistic model of the sample structure is needed [30].

4 RESULTS AND DISCUSSION

4.1 Deposition conditions

Plasma polymer films of tetravinylsilane monomer were deposited on polished silicon wafers. The substrates were pretreated with oxygen plasma (10 sccm, 5.4 Pa, 30 W, 10 min) to create a more reactive surface on silicon wafers. Tetravinylsilane films were deposited at a mass flow rate of 1.35 and 4.05 sccm (10 and 29 sccm respectively measured for N_2 mass flow meter) with monomer pressure of 3.8 and 7.6 Pa and RF power in range of $10-100$ W on 12 identical substrates placed in positions (Figure 14) A, G, N, O, U and AA on both the center, using the glass substrate holders, and the edge, where substrates are placed on the bottom wall of reaction chamber. After the deposition the reaction chamber was filled with argon gas with mass flow rate of 10 sccm for 60 min for quenching free radicals and after 24 hours the samples were removed from the reaction chamber. The samples were then measured with ellipsometer to obtain film thickness and the deposition speed was calculated based on the film thickness and the deposition time.

Table 4: List of samples and deposition conditions.

Sample	**Position in reaction chamber**		**Pretreatment**	**TVS [sccm N_2]**	**TVS pressure [Pa]**	**P [W]**	**Deposition time [min]**	**Film thickness [nm]**	**deposition speed [nm/min]**
A4033	center	A	no	10	3.84	10	4	260	65
A4034	center	G						36	9
A4035	center	N						50	13
A4036	center	O						113	28
A4037	center	U						238	60
A4038	center	AA						1040	260
A4039	edge	A						55	14
A4040	edge	G						19	5
A4041	edge	N						47	12
A4042	edge	O						76	19
A4043	edge	U						153	38
A4044	edge	AA						498	1254
A4057	center	A	yes	10	7.6	10	7	630	90
A4058	center	G						297	42
A4059	center	N						220	31
A4060	center	O						241	34
A4061	center	U						439	63
A4062	center	AA						1530	219
A4063	edge	A						78	11
A4064	edge	G						83	12
A4065	edge	N						131	19

A4066	edge	O	yes	10	7.6	10	7	204	29
A4067	edge	U						265	38
A4068	edge	AA						906	129
A4081	center	A	yes	29	3.8	10	7	1248	178
A4082	center	G						852	122
A4083	center	N						844	121
A4084	center	O						784	112
A4085	center	U						790	113
A4086	center	AA						1535	219
A4087	edge	A						979	140
A4088	edge	G						587	84
A4089	edge	N						605	86
A4090	edge	O						559	80
A4091	edge	U						617	88
A4092	edge	AA						1218	174
A4093	center	A	yes	29	3.73	30	7	747	107
A4094	center	G						364	52
A4095	center	N						901	129
A4096	center	O						606	87
A4097	center	U						833	119
A4098	center	AA						3016	431
A4099	edge	A						112	16
A4100	edge	G						222	32
A4101	edge	N						446	64
A4102	edge	O						440	63
A4103	edge	U						388	55
A4104	edge	AA						2240	320
A4105	center	A	yes	29	3.65	100	7	414	59
A4106	center	G						216	31
A4107	center	N						243	35
A4108	center	O						429	61
A4109	center	U						860	123
A4110	center	AA						3990	570
A4111	edge	A						238	34
A4112	edge	G						135	19
A4113	edge	N						X	X
A4114	edge	O						315	45
A4115	edge	U						461	66
A4116	edge	AA						2130	304
A4117	center	A	yes	29	7.64	30	7	1201	172
A4118	center	G						464	66
A4119	center	N						844	121

A4120	center	O	yes	29	7.64	30	7	760	109
A4121	center	U						940	134
A4122	center	AA						3966	567
A4123	edge	A						1046	149
A4124	edge	G						238	34
A4125	edge	N						400	57
A4126	edge	O						602	86
A4127	edge	U						608	87
A4128	edge	AA						2784	398

In the graphs below, we can observe and compare the deposition speed and film thickness along the reaction chamber based on these criteria: the difference in position of placed sample (center/edge), the difference in monomer mass flow rate, the difference in RF generator power and the difference in monomer vapour pressure.

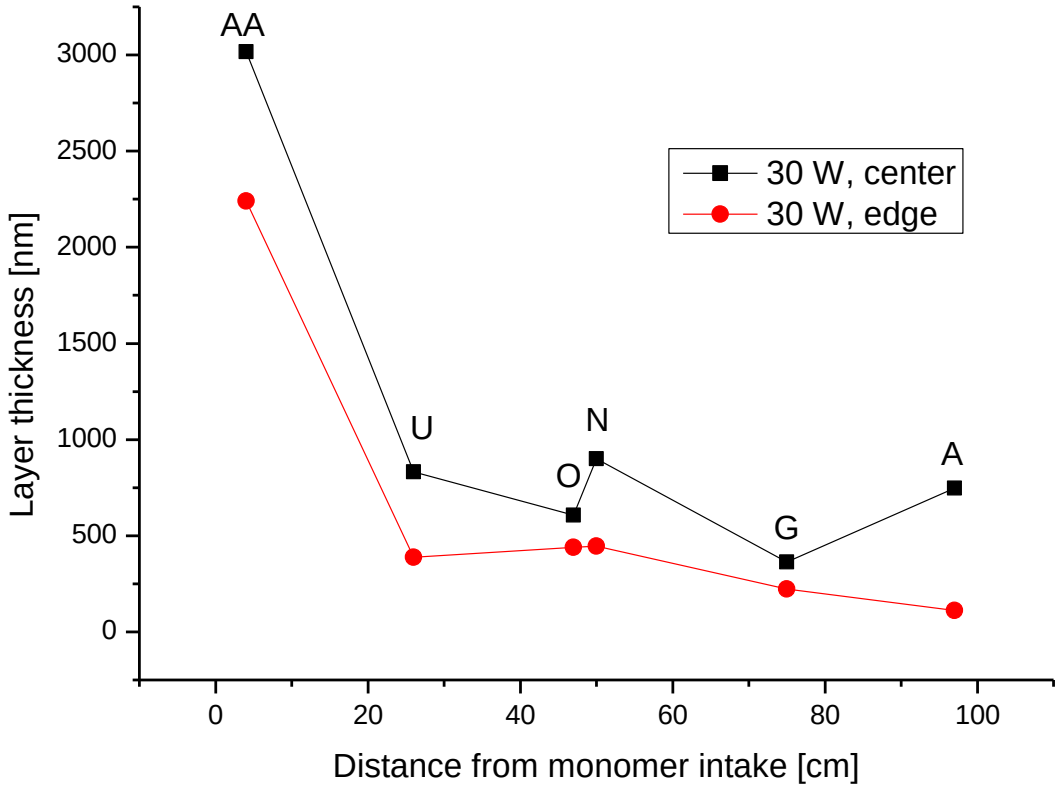

Figure 19: Difference in layer thickness in the center and on the edge of the reaction chamber.

In Figure 19 we can see that the layer thickness in the center of the reaction chamber is higher than on the edge in all positions. This is a desirable trend because we want to minimize the film thickness on the edge of reaction chamber. The highest thickness is in the position closest to the monomer intake because the concentration of monomer is the highest. The layer thickness then decreases substantially. Samples in position N, compared to other positions, are placed directly under live electrode. This causes the difference in layer thickness and

deposition speed in positions O and N and the effect may vary based on the deposition conditions. We can observe a slight increase in layer thickness of sample placed in the center in position N. The sample at the monomer outlet has increased layer thickness as well.

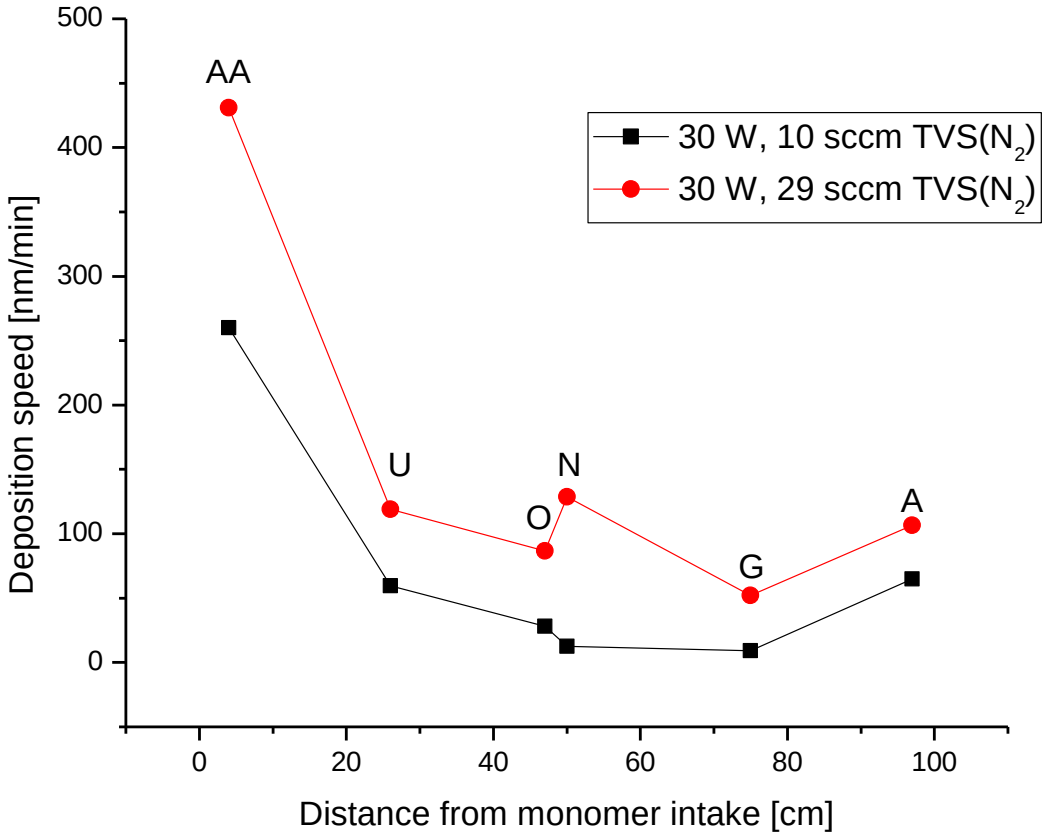

Figure 20: Deposition speed along the plasma chamber for different mass flow rates.

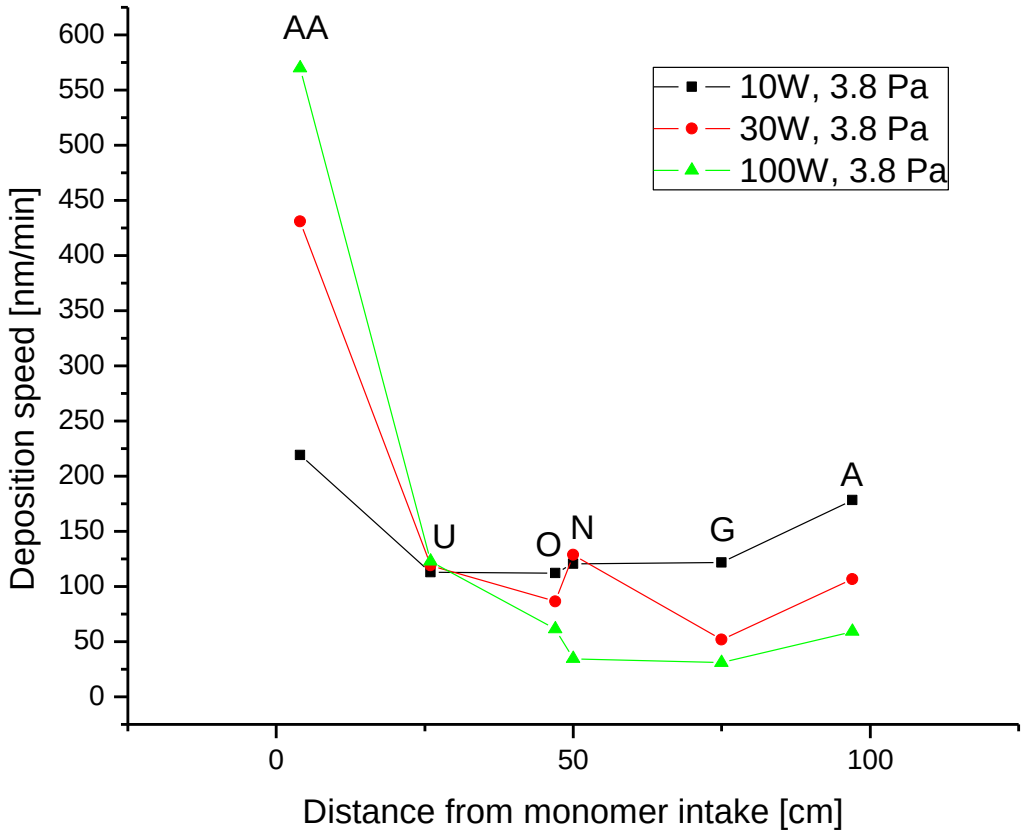

Figure 21: Deposition speed with different RF generator power at mass flow rate of 10 sccm for N_2 (1.35 sccm TVS).

Figure 20 follows the same trend as the previous graph with the highest deposition speed near the monomer intake, with slower deposition on samples in the central area of the reaction chamber and a slight increase at the end of the reaction chamber. The samples with 29 sccm for N_2 (4.05 sccm TVS) have higher deposition rates throughout the whole reaction chamber.

In Figure 21, we can see the difference in deposition speed based on different RF generator power. Samples deposited under 100 W have higher deposition speed at the start of reaction chamber but the deposition rate dwindles further in the chamber, having the lowest deposition speed at the end of the reaction chamber. Deposition speed decreases in the N position. Samples under 30 W plasma, compared to 100 W plasma have slightly lower deposition rates at the monomer inlet and slightly higher deposition speed at the monomer outlet. Position N has increased deposition speed. Samples under 10 W have the most balanced deposition speed throughout the reaction chamber. The sample in the N position has deposition speed comparable to the sample in position O.

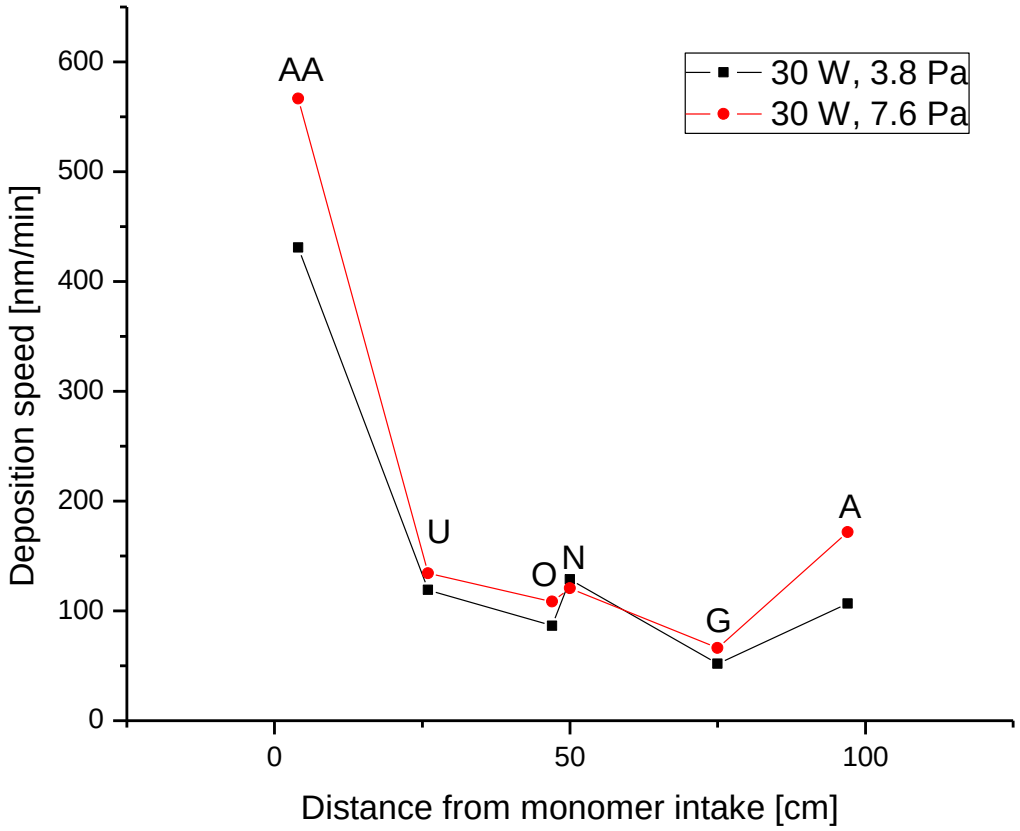

Figure 22: Deposition speed with different monomer vapour pressure at TVS mass flow rate of 10 sccm for N_2.

Figure 22 shows the impact of different monomer vapour pressure on the deposition speed. Samples with monomer pressure of 7.6 Pa have overall slightly higher deposition speed compared to 3.8 Pa. The samples in both pressure coditions have slightly increased deposition speed in the position N.

4.2 IR spectroscopy

IR spectra were obtained using the FT-IR spectroscope as well as functional groups of created plasma polymers. IR absorption bands were assigned according to Table 5 which also contains the typical wavenumber of the absorption band. Samples were chosen with the thickness about 0.1 μm.

Table 5: Functional groups and their absorption bands [31].

Wavenumber [cm^{-1}]	**Assignment**
3461	O-H stretching
2921-2894	CH_x stretching $(x = 1,2,3)$
2194-2116	Si-H stretching
1708	C=O stretching
1608	C=C stretching in vinyl
1457	CH_2 scissoring
1408	CH_2 deformation in vinyl
1266-1257	CH_2 wagging in Si-CH_2-R
1067-1056	Si-O-C stretching
1010	=CH wagging in vinyl
950	=CH_2 wagging in vinyl
885-830	Si-O bending
780-745	Si-C stretching

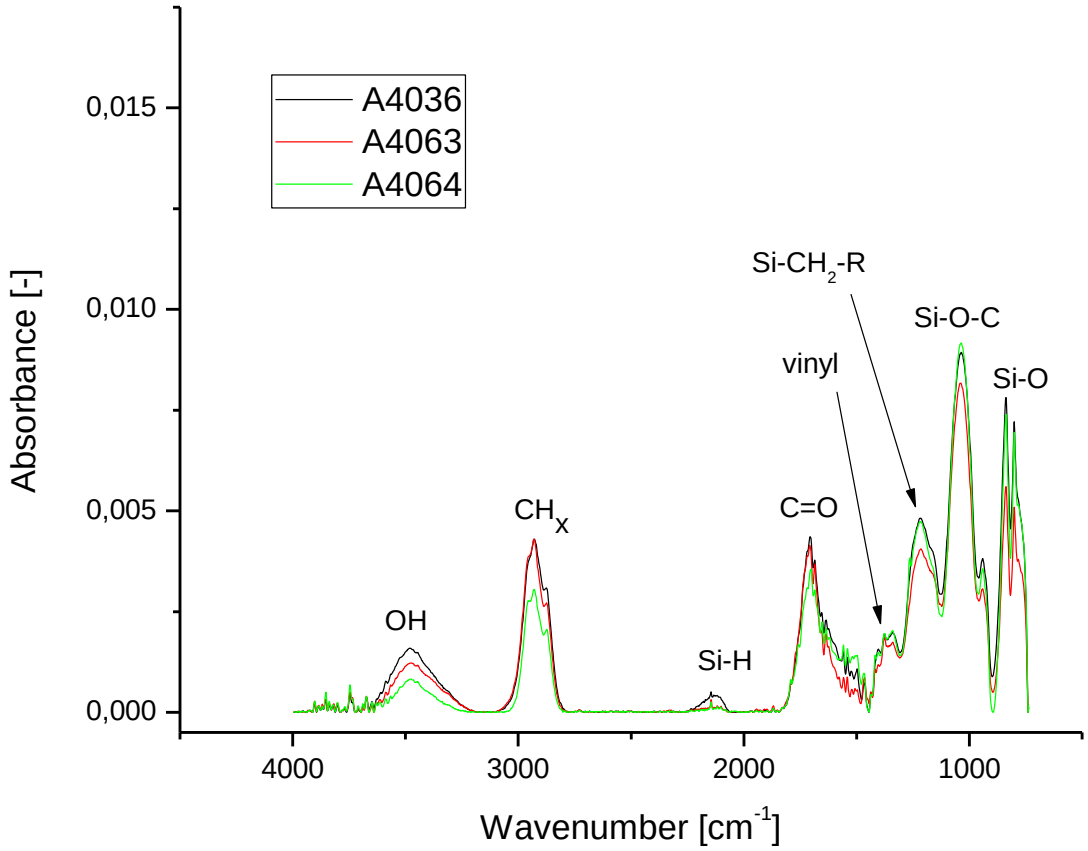

Figure 23: FT-IR spectrum of selected samples.

Figure 23 contains the measured spectra of samples with approximate layer thickness of 100 nm. The OH, C=O, Si-O-C, and Si-O groups assigned in FTIR spectra are due to aging of

the thin film, absorbing oxygen from surrounding air into the thin film matrix. The difference in the absorbance of the samples is caused by the difference in layer thickness of individual samples.

4.3 Spectroscopic ellipsometry

Optical properties were measured using spectroscopic ellipsometry and obtained values of I_s and I_c as well as ellipsometric angles Δ and ψ were evaluated using software DeltaPsi 2. A model of material was created based on expected material type, parameterization for dielectric materials, expected thickness with real structure together with obtained values of I_s and I_c are fitted and based on this model we can obtain optical properties of the sample(Figure 24).

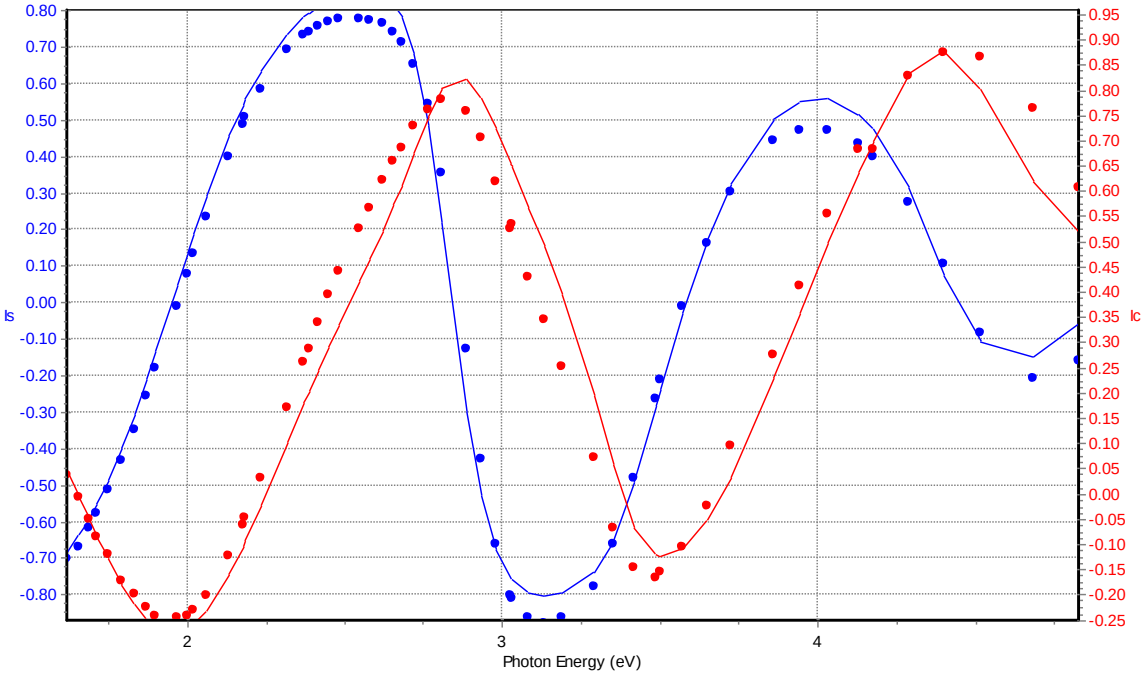

Figure 24: Model fit to measured data of sample A4106, P = 100 W.

Figure 25 shows the difference of optical properties of samples in different positions in reaction chamber within one deposition. The difference in refractive index is within the possible error of the measurement and modelling. Extinction coefficient has the most important point, where it reaches zero value. In measured samples it reaches zero at approximately the same wavelength of 400 nm and the thin film is transparent within the range of visible light. We can conclude that within one deposition in all positions of the reaction chamber.

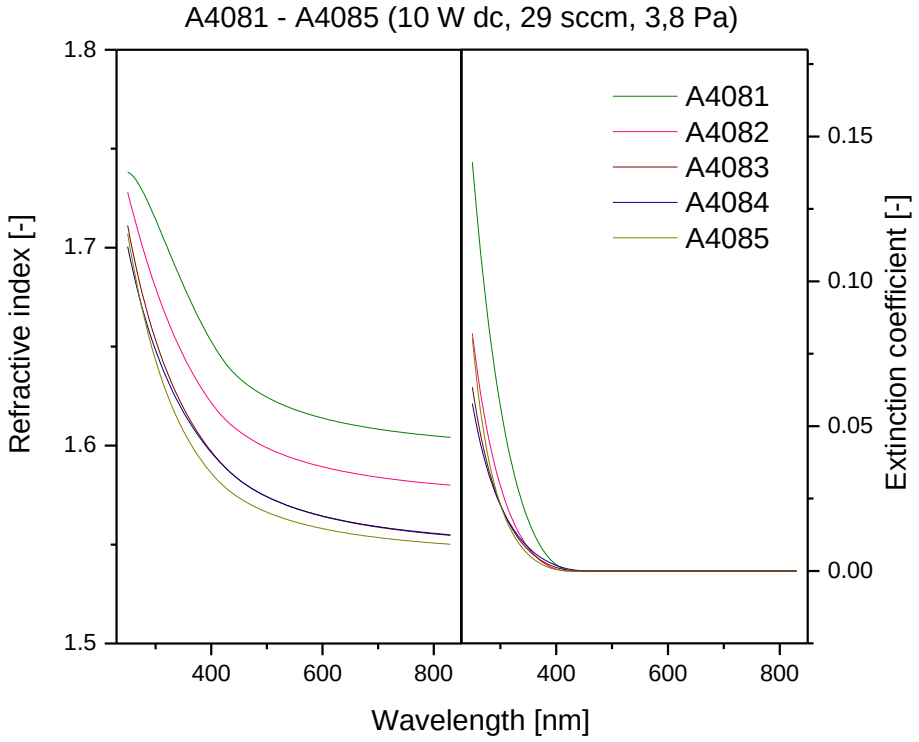

Figure 25: Graph of optical properties of samples A4081-A4085.

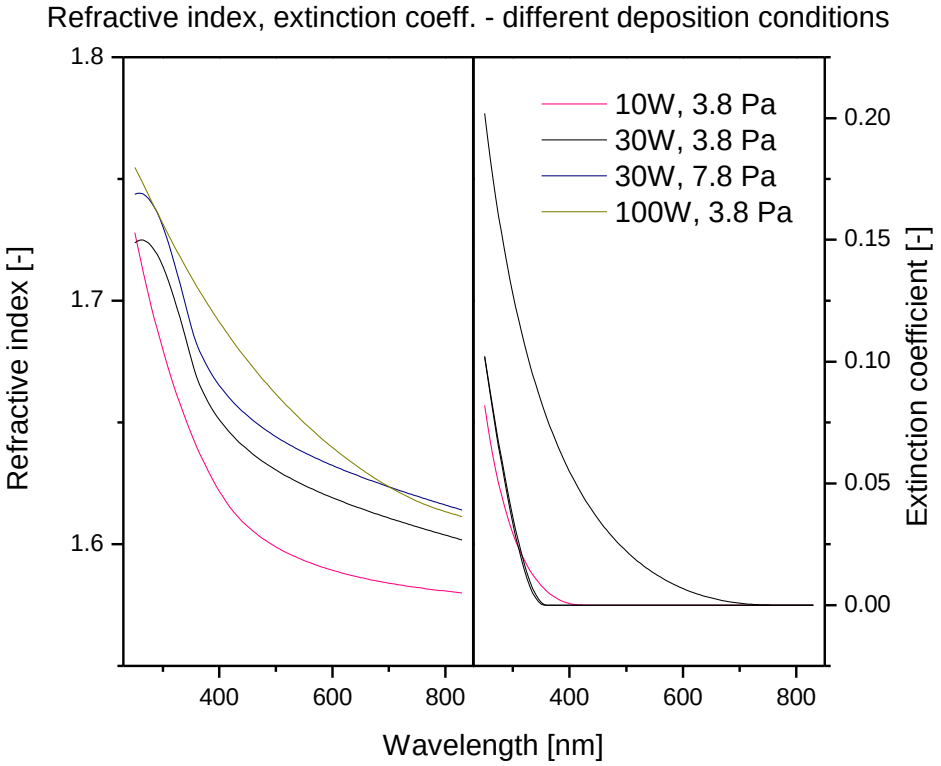

Figure 26: Graph of optical properties of samples with different deposition conditions.

Figure 26 shows that the refractive index slightly increases with higher power. The values are within the range 1.58 and 1.76. Extinction coefficient of 100 W sample reaches zero value at wavelength of approximately 700 nm, which means that the sample absorbs light throughout the visible spectrum and becomes transparent in the area of infrared spectrum. Other samples reach zero value at 350-400 nm. Samples treated with higher powered plasma have their extinction coefficient shifted to higher wavelengths.

5 CONCLUSION

The aim of the bachelor thesis was to characterize the deposition system for thin film coating and analyze the deposited films using the spectroscopic ellipsometer and IR spectrometer. All used samples are in Table 4 with respective deposition conditions, deposited layer thickness and calculated deposition speed. The data was processed into graphs comparing different deposition conditions. In Figure 19 it is possible to see that the deposition speed in the center positions is higher throughout the reaction chamber. Figure 20 contains comparison of different TVS mass flow rates. The samples deposited with 29 sccm for N_2 (4.05 sccm TVS) proved to have higher deposition speed than of the samples deposited with 10 sccm for N_2 (1.35 sccm TVS). The influence of RF power on deposition speed can be seen in Figure 21. The samples deposited with RF power of 100 W have the most unevenly distributed deposition speed, having the highest deposition rate closest to the monomer intake and the lowest deposition rate furthest of the monomer intake. Other samples follow this trend with lower RF power decreasing the deposition speed closest to the monomer intake and increasing deposition speed further away from it. Samples at position U have relatively the same deposition speed regardless of RF power. Figure 22 contains samples deposited with different monomer vapour pressure, where the samples deposited with higher monomer pressure have slightly higher deposition speed except the samples in position N, where the deposition speed of lower monomer pressure exceeds that of the higher pressure.

Using the IR spectroscopy, representative samples were selected with thin layer thickness closest to 0.1 μm. Figure 23 shows those samples and the absorption bands of functional groups present. This confirms that material with similar composition was created at different deposition conditions as well as different placements in reaction chamber.The chemical groups containing the oxygen atom are caused by the oxidation of samples exposed to air. The differences in the absorption amount of respective functional groups and their absorption bands can be caused by diverse layer thicknesses of selected samples. Further investigation is needed to find precise difference in the material based on deposition conditions.

Using spectroscopic ellipsometry, layer thickness as well as optical properties of the samples has been measured. In Figure 25Figure 26 we can see the difference in refractive index and extinction coefficient within different positions of the chamber and different deposition conditions respectively. The samples within different positions of reaction chamber with same deposition conditions experience a slight difference in refractive index with little to no difference in extinction coefficient, making the thin film of all samples transparent in visible light. The samples with different deposition conditions have a greater difference in refractive index, with increasing refractive index with increasing RF power, having the sample with RF power of 100 W the highest. Extinction coefficient of these samples has one major difference and that is in the 100 W sample, having its extinction coefficient reach value of 0 at wavelength of 700 nm, making the thin layer of this sample absorb light frequencies of the visible light.

The results of this thesis create a baseline for fibre deposition on deposition apparatus “A4” and finding the optimal deposition conditions for further depositions as well as possible improvement of the deposition system.

6 REFERENCES

[1] INAGAKI, N. *Plasma Surface Modification and Plasma Polymerization.* Lancaster:Technomic Publishing Company, 1996. ISBN 1-56676-337-1

[2] HIPPLER, R., Pfau, S., Schmidt, M., K.H, Shoenbach, Eds. *Low Temperature Plasma Physics – Fundamentals Aspects and Applications*. Berlin: Wiley-VCH, 2001

[3] YASUDA, H. *Plasma polymerization*. Academic Press, Inc., New York, 1985. ISBN 0-12-768760-2

[4] BITTENCOURT, J.A. *Fundamentals of Plasma Physics*. Third Edition. New York, NY: Springer New York, 2004. ISBN 14-757-4030-1.

[5] BIEDERMAN, Hynek. *Plasma polymer films*. London: Imperial College Press, c2004, 386 p. ISBN 1-86094-467-1.

[6] KIYOTAKA WASA, Makoto Kitabatake. *Thin film materials technology sputtering of compound materials*. Norwich, NY: William Andrew Pub, 2004. ISBN 08-155-1931-1.

[7] FREUND, L a S SURESH. *Thin film materials: stress, defect formation and surface evolution*. Cambridge: Cambridge University Press, 2003. ISBN 05-218-2281-5.

[8] SEGUI, Yvan. Plasma deposition from organosilicon monomers. In: D' AGOSTINO, R. (ed.) *Plasma processing of polymers*. Netherlands: Kluwer Academic Publishers, 1997, 305-319. ISBN 0-7923-4859-1.

[9] SEGUI, Y. a Bui AI. Gas discharge in hexamethyldisiloxane. *Journal of Applied Polymer Science*.**20**(6), 1611-1618. DOI: 10.1002/app.1976.070200618. ISSN 00218995. Dostupné také z: http://doi.wiley.com/10.1002/app.1976.070200618.

[10] WRÓBEL, A. M., M. R. WERTHEIMER, J. DIB a H. P. SCHREIBER. Polymerization of Organosilicones in Microwave Discharges. *Journal of Macromolecular Science: Part A - Chemistry*. 2006, **14**(3), 321-337. DOI: 10.1080/00222338008056716. ISSN 0022-233x. Dostupné také z: http://www.tandfonline.com/doi/abs/10.1080/00222338008056716.

[11] TAJIMA, Ichiro a Minoru YAMAMOTO. Spectroscopic study on chemical structure of plasma-polymerized hexamethyldisiloxane. *Journal of Polymer Science: Polymer Chemistry Edition*.**23**(3), 615-622. DOI: 10.1002/pol.1985.170230303. ISSN 03606376. Dostupné také z: http://doi.wiley.com/10.1002/pol.1985.170230303.

[12] AKOVALI, G. a N. HASIRCI. Polymerization of hexamethyldisiloxane by plasma on activated charcoal: Investigation of parameters. *Journal of Applied Polymer Science*. **29**(8), 2617-2625. DOI: 10.1002/app.1984.070290816. ISSN 00218995. Dostupné také z: http://doi.wiley.com/10.1002/app.1984.070290816.

[13] SACHDEV, Krishna G. a Harbans S. SACHDEV. Characterization of plasma-deposited organosilicon thin films. *Thin Solid Films*. 1983, **107**(3), 245-250. DOI: 10.1016/0040-6090(83)90403-0. ISSN 00406090. Dostupné také z: http://linkinghub.elsevier.com/retrieve/pii/0040609083904030.

[14] MUKHERJEE, S.P. a P.E. EVANS. The deposition of thin films by the decomposition of tetra-ethoxy silane in a radio frequency glow discharge. *Thin Solid Films*. 1972, **14**(1), 105-118. DOI: 10.1016/0040-6090(72)90373-2. ISSN 00406090. Dostupné také z: http://linkinghub.elsevier.com/retrieve/pii/0040609072903732.

[15] PAI, C. S., J. F. MINER a P. D. FOO. Electron Cyclotron Resonance Microwave Discharge for Oxide Deposition Using Tetraethoxysilane. *Journal of The Electrochemical Society*. 1992, **139**(3), 850-856. DOI: 10.1149/1.2069315. ISSN 00134651. Dostupné také z: http://jes.ecsdl.org/cgi/doi/10.1149/1.2069315.

[16] SELAMOGLU, N., J. A. MUCHA, D.E. IBBOTSON a D.L. FLAMM. Silicon oxide deposition from tetraethoxysilane in a radio frequency downstream reactor: Mechanisms and step coverage.*Journal of Vacuum Science*. **7**(6), 1345-1351. DOI: 10.1116/1.584536. ISSN 0734211x. Dostupné také z: http://scitation.aip.org/content/avs/journal/jvstb/7/6/10.1116/1.584536.

[17] ISHII, Keisuke, Yoshimichi OHKI a Hiroyuki NISHIKAWA. Optical characteristics of SiO2 formed by plasma-enhanced chemical-vapor deposition of tetraethoxysilane. *Journal of Applied Physics*. 1994, **76**(9), 5418-5422. DOI: 10.1063/1.357196. ISSN 00218979. Dostupné také z: http://scitation.aip.org/content/aip/journal/jap/76/9/10.1063/1.357196.

[18] INAGAKI, N., S. KONDO a T. MURAKAMI. Preparation of siloxane-like films by glow discharge polymerization. *Journal of Applied Polymer Science*. **29**(11), 3595-3605. DOI: 10.1002/app.1984.070291133. ISSN 00218995. Dostupné také z: http://doi.wiley.com/10.1002/app.1984.070291133.

[19] RAU, C. a W. KULISCH. Mechanisms of plasma polymerization of various silico-organic monomers. *Thin Solid Films*. 1994, **249**(1), 28-37. DOI: 10.1016/0040-6090(94)90081-7. ISSN 00406090. Dostupné také z: http://linkinghub.elsevier.com/retrieve/pii/0040609094900817.

[20] NGUYEN, V. S., J. UNDERHILL, S. FRIDMANN a P. PAN. Plasma Organosilicon Polymers. *Journal of The Electrochemical Society*. 1985, **132**(8), 1925-1932. DOI: 10.1149/1.2114255. ISSN 00134651. Dostupné také z: http://jes.ecsdl.org/cgi/doi/10.1149/1.2114255.

[21] INAGAKI, N., S. KONDO, M. HIRATA a H. URUSHIBATA. Plasma polymerization of organosilicon compounds. *Journal of Applied Polymer Science*. **30**(8), 3385-3395. DOI: 10.1002/app.1985.070300821. ISSN 00218995. Dostupné také z: http://doi.wiley.com/10.1002/app.1985.070300821.

[22] CECH, V., J. STUDYNKA, N. CONTE a V. PERINA. Physico-chemical properties of plasma-polymerized tetravinylsilane. *Surface and Coatings Technology*. 2007, **201**(9-11), 5512-5517. DOI: 10.1016/j.surfcoat.2006.07.086. ISSN 02578972. Available at: http://linkinghub.elsevier.com/retrieve/pii/S0257897206006852.

[23] GÜNZLER, Helmut a Hans-Ulrich GREMLICH. *IR Spectroscopy: An Introduction*. Berlin: Wiley-VCH, 2002. ISBN 3-527-28896-1.

[24] NORMAN B. COLTHUP, Norman B.Lawrence H. *Introduction to infrared and Raman spectroscopy*. 2d ed. New York: Academic Press, 1975. ISBN 03-231-6160-X.

[25] LINDON, John C. *Encyclopedia of spectroscopy and spectrometry*. 2nd ed. Amsterdam: Elsevier, 2010. ISBN 01-237-4413-X.

[26] KLÍČ, Alois, Karel VOLKA a Miroslava DUBCOVÁ. *Fourierova transformace s příklady z infračervené spektroskopie*. Vyd. 3. Praha: Vysoká škola chemicko-technologická, 2002. ISBN 80-708-0478-5.

[27] FUJIWARA, Hiroyuki. *Spectroscopic ellipsometry principles and applications*. Chichester, England: John Wiley, 2007. ISBN 04-700-6018-2.

[28] JOBIN, Ywon S.A.S *Spectroscopic ellipsometry*. Příručka k spektroskopickému fázově modulovanému elipsometru UVISEL.

[29] BRUKER OPTIK GmbH, *VERTEX 80v User Manual*. 1st edition 2006. D-76275

[30] SAM ZHANG (ed.). *Nanostructured Thin Films and Coatings. Mechanical Properties*. Hoboken: CRC Press, 2010. ISBN 14-200-9403-3.

[31] CECH, Vladimir, Jan STUDYNKA, Filip JANOS a Vratislav PERINA. Influence of Oxygen on the Chemical Structure of Plasma Polymer Films Deposited from a Mixture of Tetravinylsilane and Oxygen Gas. *Plasma Processes and Polymers*. 2007, **4**(S1), S776-S780. DOI: 10.1002/ppap.200731903. ISSN 16128850. Dostupné také z: http://doi.wiley.com/10.1002/ppap.200731903

7 LIST OF USED ABBREVIATIONS AND SYMBOLS

BTMSM	bis(trimethylsilyl)methane
DVTMDSO	divinyltetramethyldisiloxane
FIR	far infrared
FT-IR	Fourier transform infrared
HMDS	hexamethyldisilane
HMDSN	hexamethyldisilazane
HMDSO	hexamethyldisiloxane
HTP	high-temperature plasma
IR	infrared
LTP	low-temperature plasma
NIR	near infrared
OMCATS	octamethylcyclotetrasiloxane
PECVD	plasma enhanced chemical vapour deposition
PME	photoelastic modulator ellipsometer
PSD	polarization state detector
PSG	polarization state generator
RAE	rotating analyser ellipsometer
sccm	standard cubic centimetre per minute
TEOS	tetraethoxysilane
TMDSO	tetramethyldisiloxane
TMOS	methyltrimethoxysilane
TMS	tetramethylsilane
TVS	tetravinylsilane
A_T	Tauc constant
E_0	peak transition energy
E_g	optical band gap
I_0	intensity of monochromatic radiation entering a sample
I	intensity transmitted by the sample
N_D	number of charged particles
n_e	concentration of electrons
P	Cauchy principal part
P_{eff}	effective power
T_e	electron energy
T_i	ion energy
T_g	translational kinetic energy of gas
λ_D	Debye length
ω	angular frequency of typical plasma oscillation
ε_1(E)	real part of the dielectric function
ε_2 (E)	imaginary part of the dielectric function
ε_1^{∞}	fitting parameter
Γ	broadening term